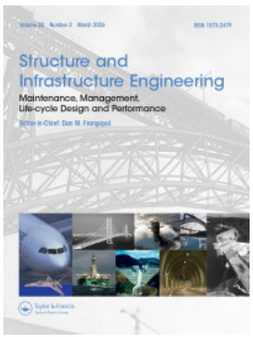

Taylor & Francis
Taylor & Francis Group

Structure and Infrastructure Engineering
Maintenance, Management, Life-Cycle Design and Performance

ISSN: 1573-2479 (Print) 1744-8980 (Online) Journal homepage: www.tandfonline.com/journals/nsie20

A novel framework for assessing the serviceability of footbridges under human-induced bending and torsional vibrations: from detailed formulation to simplified design method

Ghita Eslami Varzaneh, Elisa Bassoli, Loris Vincenzi, Angelo Aloisio, Bruno Briseghella & Roberto Tomasi

To cite this article: Ghita Eslami Varzaneh, Elisa Bassoli, Loris Vincenzi, Angelo Aloisio, Bruno Briseghella & Roberto Tomasi (18 Jan 2026): A novel framework for assessing the serviceability of footbridges under human-induced bending and torsional vibrations: from detailed formulation to simplified design method, Structure and Infrastructure Engineering, DOI: 10.1080/15732479.2026.2612946

To link to this article: https://doi.org/10.1080/15732479.2026.2612946

Published online: 18 Jan 2026.

STRUCTURE AND INFRASTRUCTURE ENGINEERING
https://doi.org/10.1080/15732479.2026.2612946

A novel framework for assessing the serviceability of footbridges under human-induced bending and torsional vibrations: from detailed formulation to simplified design method

Ghita Eslami Varzaneh[a], Elisa Bassoli[a], Loris Vincenzi[a], Angelo Aloisio[b], Bruno Briseghella[c] and Roberto Tomasi[d]

[a]Department of Engineering "Enzo Ferrari", University of Modena and Reggio Emilia, Modena, Italy; [b]Department of Civil, Construction-Architectural and Environmental Engineering, University of L'Aquila, L'Aquila, Italy; [c]College of Civil Engineering, Fuzhou University, Fuzhou, China; [d]Faculty of Science and Technology, Norwegian University of Life Sciences, Oslo, Norway

ABSTRACT

Modern footbridges are highly susceptible to dynamic vibrations induced by pedestrians. While significant research has focused on vertical and lateral vibrations generated by walking, the effects of vertical forces on torsional vibrations remain insufficiently addressed. Traditional assessment methods generally overlook torsional dynamics, which can be limiting under eccentric pedestrian loading activating torsional modes. This oversight may lead to inaccuracies in evaluating structural performance, particularly for complex footbridges where torsional effects play a significant role. This paper presents a detailed numerical modelling approach incorporating both translational and rotational effects induced by pedestrian excitation, acknowledging the coupling between bending and torsion in vertical vibrations. Numerical analyses are conducted involving individuals walking with parametrically varied eccentricities and crowd flows simulated at the microscale, to evaluate the structural response under various loading scenarios. A simplified design-oriented method to account for coupled bending-torsional vibrations is also introduced, based on multiplication factors enabling traditional bending-only analyses to be easily adjusted to include torsional effects. The proposed method is validated through experimental testing conducted on a boomerang-shaped footbridge with asymmetrical cross-section, subjected to single pedestrians walking eccentrically. Results confirm the method accuracy and highlight the importance of considering bending and torsional dynamics for reliable serviceability assessments.

ARTICLE HISTORY
Received 26 August 2025
Revised 5 November 2025
Accepted 22 November 2025

KEYWORDS
Asymmetric bridges; crowd loading; experimental validation; footbridge design; pedestrian-induced vertical vibrations; serviceability assessment; structural dynamics; torsional effects

1. Introduction

Pedestrians are a well-recognised source of dynamic vibrations in lightweight architectural designs, such as modern footbridges (Van Nimmen et al., 2014). These structures are particularly susceptible to human-induced excitation due to their slenderness and flexibility, resulting in low natural frequencies that may align with pedestrian walking frequencies. This can lead to potential near-resonances between the structure and human-induced excitation, making the serviceability assessment a critical consideration in the design and evaluation of modern footbridges (Li et al., 2025; Lievens et al., 2018; Rodríguez-Suesca et al., 2022; Van Nimmen et al., 2017). The force generated by walking varies over time and space, with components in the vertical, horizontal-lateral, and horizontal-longitudinal directions (Bachmann & Ammann, 1987). Among these, the vertical component is dominant in magnitude and potentially constitutes the primary source in generating torsional vibrations.

The serviceability assessment of slender footbridges has traditionally focused on evaluating flexural responses driven by bending modes, as these are typically the dominant contributors to vertical vibrations. However, especially in the presence of geometric or load asymmetries, torsional modes or mixed bending-torsional modes may be activated, with the interaction between bending and torsion complicating the overall structural response. In such cases, overlooking torsional effects can lead to significant errors in serviceability evaluations, as torsion-induced rotations directly affect vertical vibrations, particularly at locations farther from the structure centre of mass.

While significant research has been conducted on vertical and lateral walking forces (Ingólfsson et al., 2012; Racic et al., 2009; Venuti & Tubino, 2021; Živanović et al., 2005), less attention has been given to walking-induced torsional effects. Specialised studies have explored moments in biomechanics (e.g. gait analysis) (Fukuchi et al., 2019; Lu & Chang, 2012); however, these studies primarily focus on knee and ankle movements, rather than the impact of eccentric vertical forces on the structural dynamics. Indeed, human-induced torsional effects may couple with flexural vibrations, amplifying dynamic responses and posing risks to the structural performance. Despite the growing recognition of torsional dynamics in the

CONTACT Elisa Bassoli elisa.bassoli@unimore.it Department of Engineering "Enzo Ferrari", University of Modena and Reggio Emilia, Modena, Italy.

design of modern footbridges, the research addressing this aspect is still sparse, highlighting a critical gap in the literature (Bruno et al., 2012; Eslami Varzaneh et al., 2025).

Notwithstanding the clear implications for structural serviceability, current codes of practice neglect the torsional effects of the pedestrian action (BSI, 2008; HIVOSS, 2008; ISO 10137, 2007; SETRA, 2006). This oversight extends to numerical studies, which predominantly focus on vertical pedestrian forces and the resulting flexural vibrations, while largely overlooking how such forces may also induce torsional responses (da Silva et al., 2013; Jiménez-Alonso et al., 2016; Venuti et al., 2016; Živanović et al., 2010). Similarly, serviceability-focused experimental investigations are typically not supported by numerical models incorporating the human-induced torsion. This limitation applies not only to simple, straight footbridges (Brownjohn et al., 2004; Van Nimmen et al., 2021), but also for more geometrically complex structures, such as those with curved or asymmetrical layouts that exhibit bending-torsional modes within the typical range of pedestrian pacing frequencies (Bassoli, Gambarelli, et al., 2018; Chen et al., 2024; Zhang et al., 2021). Such irregular designs are increasingly common in modern architecture and engineering (Al-Smadi et al., 2022; Bursi et al., 2014; Caetano et al., 2010; Fenu et al., 2019; He et al., 2022; Miyachi & Nakamura, 2021; Roda-Casanova et al., 2024), further emphasising the need for a deeper understanding of pedestrian-induced torsional effects.

In summary, while vertical bending modes dominate current serviceability evaluations, ignoring torsional effects could limit the accuracy of assessments in certain footbridges, particularly those with non-symmetric designs and/or subject to eccentric loading conditions which may trigger torsional modes. Addressing these issues requires a more detailed approach to numerical modelling, including both the translational and rotational components of the structure motion, and representing pedestrians not only as vertical forces but also as moments arising from these vertical forces.

Within this framework, this paper introduces a generalised approach designed to capture the interaction between bending and torsion in vertical vibrations caused by human excitation, addressing the complex nature of these combined responses. Special attention is given to the influence of both isolated pedestrians and pedestrian crowds, as these represent two fundamentally different excitation scenarios. While a single pedestrian walking eccentrically and/or on an asymmetric structural layout is expected to induce significant torsional effects due to a non-zero moment arm with respect to the structure centre of mass, in a crowd scenario, opposing moment arms from multiple individuals may lead to partial or full cancellation of these torsional contributions. This suggests that (counter-intuitively) torsional effects could decrease as crowd density increases. However, this cancellation may not occur when the structure is geometrically asymmetric or presents non-symmetric behaviour. These expectations motivate the decision to investigate both single pedestrian and sparse-to-dense crowd-loading cases, to better understand the footbridge torsional vibrations induced by walking.

To this end, the proposed method is first validated through experimental testing. A full-scale test is conducted on a boomerang-shaped footbridge located in Oslo (Norway) (Mo et al., 2019), characterised by an asymmetrical cross-section, where individuals of varying age and body mass walk eccentrically across the structure to deliberately induce torsional actions and activate corresponding reactions. After validating the method on the specific experimental application, further numerical simulations are carried out for single pedestrians walking along eccentrically varied trajectories, to allow a parametric investigation of the torsion-induced dynamic response. Also, pedestrian traffic scenarios with increasing density are simulated, to evaluate how the inclusion (or omission) of torsional effects influences serviceability assessments across different usage levels.

Lastly, a simplified design-stage method based on torsional and positional multiplication factors is proposed to enable fast and practical assessments without ignoring critical torsion-bending interactions. The multiplication factors are derived mathematically by comparing the modal equations of motion with one (bending-related displacement) and two (bending-related displacement and torsion-related rotation) degrees of freedom. These multiplication factors incorporate only modal characteristics and eccentricities linked to structure and loading, which enables their calculation a-priori. As a result, they represent a meaningful metric for predicting the effect of torsional dynamics without the need for explicitly computing the coupled bending-torsional response. Indeed, the simplified method allows rapid serviceability checks by operating within a traditional bending-only framework, which provides the response of the examined section at its centre of mass, assuming rigid translation. It then adjusts the computed vibration response to account for the torsional influence on bending vibrations at the centre of mass, recognising that rotational effects may either amplify or attenuate the response there. In addition, a further adjustment is applied to forecast the response at cross-sectional locations situated away from the centre of mass, since the peak acceleration does not typically occur at the centre of mass when torsional-related rotations are involved.

The paper is organised as follows. Section 2 introduces serviceability assessments, including the traditional background focusing on vertical bending vibrations (Section 2.1) and the generalised approach developed to account for the combined effects of torsional and flexural vibrations induced by pedestrians (Section 2.2). Section 3 describes the experimental validation of the proposed bending-torsion serviceability assessment method on a full-scale footbridge, including a description of the test setup (Section 3.1) and a comparison between experimental data and method numerical predictions related to the specific test case (Section 3.2). Section 4 deals with additional parametric numerical simulations, used for comparison between the traditional and proposed methods in serviceability evaluations, including: single pedestrians following paths with different eccentricities (Section 4.1) and crowds with free-to-congested traffic densities (Section 4.2). Section 5 derives and validates torsional and positional multiplication factors to facilitate simplified design-stage assessments. Finally, Section 6 summarises the key findings and outlines directions for future research.

2. Mathematical framework for structural vertical vibration analysis

This section presents the mathematical formulation underlying the analysis of human-induced vertical vibrations in pedestrian bridges. Section 2.1 covers the traditional framework, which considers pedestrians as vertical forces and the associated structural vertical displacements. Section 2.2 introduces an extended approach that accounts for both vertical forces and the corresponding induced moments, leading to footbridge vertical vibrations resulting from a combination of displacements and rotations. Since the proposed extension is generalised to handle coupled vibrations, it can be applied to evaluate the vibration contribution of any vertical mode, including pure bending, coupled bending-torsional, and pure torsional modes.

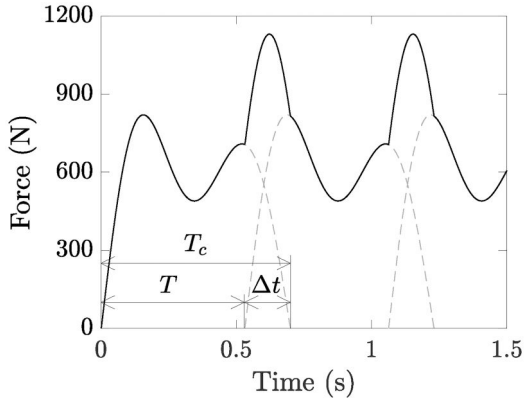

Figure 1. Step-by-step force model proposed by Li et al. (2010): periodic single-step forces, shown as grey dashed lines, and overall force, represented by a solid black line.

2.1. Traditional background for bending vibrations

The structural response to pedestrian loading is traditionally calculated using Euler-Bernoulli beam theory, which assumes that the structure behaves as a linear elastic beam under bending. Considering only the vertical displacement and its associated deflection with no torsional rotation or transverse deformation, the equation of motion for the dynamic system reads:

$$\boldsymbol{M_w}\ddot{\boldsymbol{w}}\,(t) + \boldsymbol{C_w}\dot{\boldsymbol{w}}\,(t) + \boldsymbol{K_w}\boldsymbol{w}(t) = \boldsymbol{P_w}(t) \tag{1}$$

where $\boldsymbol{M_w}$, $\boldsymbol{C_w}$ and $\boldsymbol{K_w}$ are the mass, damping and stiffness matrices, respectively, of size $n \times n$, where n is the number of beam discrete nodes; $\boldsymbol{w}(t)$ is the $n \times 1$ vector of vertical displacements at time t; $\boldsymbol{P_w}(t)$ is the $n \times 1$ pedestrian load acting on the beam over time.

In modal analysis, the displacement $\boldsymbol{w}(t)$ is expressed as a sum of contributions from the beam natural modes of vibration:

$$\boldsymbol{w}(t) = \Phi_{\boldsymbol{w}}\boldsymbol{q}(t) \tag{2}$$

where $\Phi_{\boldsymbol{w}}$ is the $n \times m$ matrix containing the mode shapes, with m being the number of modes, and $\boldsymbol{q}(t)$ is the $m \times 1$ vector of modal coordinates, which describes how the amplitude of the m modes varies with time.

By substituting the modal expansion (Equation (2)) into the equation of motion (Equation (1)) and exploiting the orthogonality of the mode shapes, the complex system is decoupled into a set of independent second-order ordinary differential equations, each representing the behaviour of a single mode. These equations describe the dynamic response $q_j(t)$ of each mode j as a single-degree-of-freedom system with its own mode shape $\phi_{\boldsymbol{w},\boldsymbol{j}}$, circular frequency ω_j, damping ratio ξ_j, modal mass $M_j = \phi_{\boldsymbol{w},\boldsymbol{j}}{}^{\mathrm{T}}\boldsymbol{M_w}\phi_{\boldsymbol{w},\boldsymbol{j}}$ and generalised external force $P_j(t) = \phi_{\boldsymbol{w},\boldsymbol{j}}{}^{\mathrm{T}}\boldsymbol{P_w}(t)$:

$$\ddot{q}_j(t) + 2\xi_j\omega_j\dot{q}_j(t) + \omega_j^2 q_j(t) = \frac{P_j(t)}{M_j} \tag{3}$$

Once each mode of interest is treated as a single-degree-of-freedom system (Equation (3)), modal coordinates are translated back to physical displacement through modal superposition (Equation (2)), summing the contributions of each mode to reconstruct the total structural response.

As concerns pedestrian loading, this paper adopts the single-step model proposed by Li et al. (2010), which formulates the footfall force $P_i(t)$ using a Fourier series:

$$P_i(t) = G_p \sum_{k=1}^{5} DLF_k \sin\left(\frac{\pi k}{T_c}t\right) \quad 0 \le t \le T_c \tag{4}$$

where i indicates the footstep, G_p is the subject weight, k is the 1-to-5 harmonic counter, DLF_k is the k-th dynamic load factor, and T_c is the foot-ground contact time. According to Li et al. (2010), dynamic load factors DLF_k and contact time T_c are pacing frequency dependent. Once the step force $P_i(t)$ is defined, the periodic walking time history $P(t)$ is constructed by replicating it with period T. This process results in an overlapping time Δt between the steps taken by the left and right feet, as illustrated in Figure 1. In this, the pacing frequency f_s can be evaluated based on the velocity v_s. Here, the cubic equation proposed by Bruno and Venuti (2008) is adopted:

$$f_s = 0.35v_s^3 - 1.59v_s^2 + 2.93v_s \tag{5}$$

Therefore, step parameters are evaluated as $T = 1/f_s$, $T_c = T/0.76$ and $\Delta t = 0.24T_c$, in line with Li et al. (2010). Following the determination of the pacing frequency f_s, the dynamic load factors DLF_k can also be obtained, using the formulation offered by Li et al. (2010):

$$DLF_k = a_k f_s + b_k \quad (k = 1, \ldots, 5) \tag{6}$$

where f_s is expressed in Hz, and coefficients a_k and b_k are listed in Table 1 for the relevant harmonics (k from 1 to 5).

Step forces are applied at T time increments and $l_s = v_s/f_s$ space increments, where l_s indicates the step length. Switching from a nodal force projection to a direct summation of step forces, the modal force can alternatively be calculated by weighting each i-th step force by the amplitude of the mode shape at the exact position where the foot is placed:

$$P_j(t) = \sum_i \phi_{w,j,i}\; P_i(t) \tag{7}$$

where $\phi_{w,j,i}$ is the j-th mode shape component evaluated at footfall location i.

2.2. Extension to coupled bending-torsional vibrations

In combined bending and torsional vibrations, the vertical displacement of any point of the cross-section depends not only on the bending-induced deflection but also on the vertical component introduced by the torsional rotation (see Figure 2). In this scenario, points on the cross-section experience varying vertical displacements, necessitating two degrees of freedom to account for both bending-related displacement and torsional rotation, assuming no transverse deformation.

Building on this, the equation of motion describes a system of n discrete nodes, each including the vertical translation due to bending and the rotational movement due to torsion:

$$\boldsymbol{M}\,\ddot{\boldsymbol{W}}(t) + \boldsymbol{C}\,\dot{\boldsymbol{W}}(t) + \boldsymbol{K}\boldsymbol{W}(t) = \boldsymbol{R}(t) \tag{8}$$

where: $\boldsymbol{W}(t)$ is a $2n \times 1$ column vector representing the generalised movements (displacements $\boldsymbol{w}$ and rotations $\boldsymbol{\theta}$) at the n nodes; $\boldsymbol{M}$ is the $2n \times 2n$ generalised mass matrix, representing how the mass is distributed across the nodes, accounting for inertia in both translational ($\boldsymbol{M_w}$) and rotational ($\boldsymbol{M_\theta}$) movements; $\boldsymbol{C}$ is the $2n \times 2n$ generalised damping matrix, modelling the energy dissipation within the system incorporating both translational ($\boldsymbol{C_w}$) and rotational ($\boldsymbol{C_\theta}$) components; $\boldsymbol{K}$ is the $2n \times 2n$ generalised stiffness matrix, defining the relationship between forces/moments ($\boldsymbol{K_w}$) and displacements/rotations ($\boldsymbol{K_\theta}$) at each node; $\boldsymbol{R}(t)$ is the $2n \times 1$ generalised external load vector acting on the beam, which includes forces corresponding to displacement degrees of freedom and moments corresponding to rotation degrees of freedom. In this, the human-induced moment can be determined by multiplying the pedestrian force vector $\boldsymbol{P_w}(t)$ $(n \times 1)$ by the moment arm vector $\boldsymbol{d_\theta}$ $(n \times 1)$, where each component of $\boldsymbol{d_\theta}$ represents the distance from the corresponding nodal force application point to the structure centre of mass:

Table 1. DLF coefficients after Li et al. (2010).

	$1.6\,\text{Hz} \le f_s \le 2.32\,\text{Hz}$		$2.32\,\text{Hz} < f_s \le 2.4\,\text{Hz}$	
	a_k	b_k	a_k	b_k
$k = 1$	−0.0698	+1.211	−0.1784	+1.463
$k = 2$	+0.1052	−0.1284	−0.4716	+1.210
$k = 3$	+0.3002	−0.1534	−0.0118	+0.5703
$k = 4$	+0.0416	−0.0288	−0.2600	+0.6711
$k = 5$	−0.0275	+0.0608	−0.0906	−0.2132

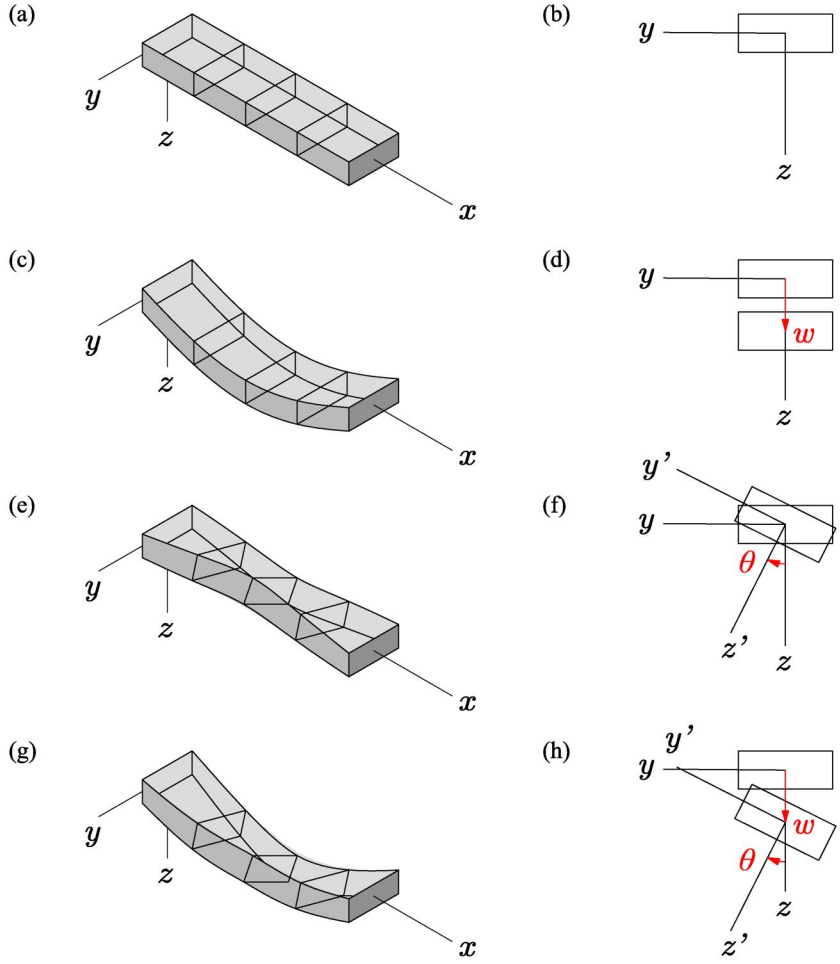

Figure 2. Simply supported beam: in undeformed condition (a and b), subject to pure bending (c and d), pure torsion (e and f), and a combination of bending and torsion (g and h); the left column illustrates the entire beam, while the right column focuses on the mid-span cross-section, with motion governed by vertical displacement w and/or rotation θ.

$$\boldsymbol{R}(t) = \begin{bmatrix} \boldsymbol{P_w}(t) \\ \mathrm{diag}(\boldsymbol{P_w}(t))\boldsymbol{d_\theta} \end{bmatrix} \tag{9}$$

Here, $\mathrm{diag}(\boldsymbol{P_w}(t))$ $(n \times n)$ indicates the square matrix with the entries of $\boldsymbol{P_w}(t)$ along the main diagonal.

Applying modal decomposition, the equation of motion is separated into components that correspond to each mode. The system is therefore reduced to independent single degrees of freedom (modes) characterised by their own amplitudes over time. The relationship can be expressed as:

$$\boldsymbol{W}(t) = \Phi \boldsymbol{Q}(t) \tag{10}$$

implying:

$$\begin{bmatrix} \boldsymbol{w}(t) \\ \boldsymbol{\theta}(t) \end{bmatrix} = \begin{bmatrix} \Phi_{\boldsymbol{w}} \\ \Phi_{\boldsymbol{\theta}} \end{bmatrix} \begin{bmatrix} Q_1(t) \\ \vdots \\ Q_m(t) \end{bmatrix} \tag{11}$$

where Φ is a $2n \times m$ matrix, with m being the number of contributing modes, including the mode shape matrices for displacements $\Phi_{\boldsymbol{w}}$ and rotations $\Phi_{\boldsymbol{\theta}}$, each of size $n \times m$. $\boldsymbol{Q}(t)$ is the modal amplitude vector of size $m \times 1$, where $Q_j(t)$ corresponds to the amplitude of the j-th mode (with $j = 1, \ldots, m$).

Following the same procedure as presented in Section 2.1, applying the modal expansion and the orthogonality of mode shapes, the original system is decoupled into a set of independent second-order ordinary differential equations, one for each mode j:

$$\ddot{Q}_j(t) + 2\xi_j \omega_j \dot{Q}_j(t) + \omega_j^2 Q_j(t) = \frac{R_j(t)}{M_j^*} \tag{12}$$

where the modal mass is calculated based on the translational mass $\boldsymbol{M_w}$ and rotational mass $\boldsymbol{M_\theta}$, correspondingly weighted by the mode shape for displacements $\phi_{\boldsymbol{w,j}}$ and rotations $\phi_{\boldsymbol{\theta,j}}$, as:

$$M_j^* = {\phi_{\boldsymbol{w,j}}}^{\mathrm{T}} \boldsymbol{M_w} \phi_{\boldsymbol{w,j}} + {\phi_{\boldsymbol{\theta,j}}}^{\mathrm{T}} \boldsymbol{M_\theta} \phi_{\boldsymbol{\theta,j}} \tag{13}$$

The modal generalised force can be calculated by projecting Equation (9) onto the modal basis:

$$R_j(t) = {\phi_{\boldsymbol{w,j}}}^{\mathrm{T}} \boldsymbol{P_w}(t) + {\phi_{\boldsymbol{\theta,j}}}^{\mathrm{T}} \left(\mathrm{diag}(\boldsymbol{P_w}(t))\boldsymbol{d_\theta}\right) \tag{14}$$

Since the pedestrian force $P(t)$ is the sum of each i-th step force (described in Equation (4)), applied at locations which generally do not coincide with the n finite element nodes, the mode shapes $\phi_{\boldsymbol{w,j}}$ and $\phi_{\boldsymbol{\theta,j}}$, originally defined at the nodes, are interpolated at these footfall positions. This ensures that the modal force accurately reflects the spatial distribution of the step loads and their associated moment arms. With this interpolation from nodes to footfall locations, the modal force is evaluated as:

$$R_j(t) = \sum_i \phi_{w,j,i}\ P_i(t) + \sum_i \phi_{\theta,j,i}\ P_i(t) d_i \tag{15}$$

In this formulation, each i-th step force $P_i(t)$ is weighted by the interpolated bending mode $\phi_{w,j,i}$ and by the torsional mode $\phi_{\theta,j,i}$ scaled by the moment arm d_i, calculated as the offset between the i-th foot position and the structure centre of mass. This allows both force and moment effects to be properly accounted for in the modal force $R_j(t)$.

Once the modal amplitude $Q_j(t)$ is determined, displacements and rotations can be computed from the mode shapes:

$$\begin{bmatrix} \boldsymbol{w_j}(t) \\ \boldsymbol{\theta_j}(t) \end{bmatrix} = \begin{bmatrix} \phi_{\boldsymbol{w,j}} \\ \phi_{\boldsymbol{\theta,j}} \end{bmatrix} Q_j(t) \tag{16}$$

The vertical displacement at a generic point H along the cross-section, at a distance e from the centre of mass, is then calculated as follows:

$$W_{H,j} = w_j + \theta_j e \tag{17}$$

Similarly, the velocities (translational and rotational) and accelerations (translational and rotational) can be obtained by substituting the first and second time derivatives of $Q_j(t)$ into Equation (16), and then combining them to obtain the overall vertical response in terms of velocity or acceleration through Equation (17).

In summary, this methodology allows for the accurate determination of vertical responses (displacements, velocities, or accelerations) at any location along the cross-section by incorporating both bending and torsional action and reaction contributions. The only required inputs are the pedestrian loading, the position of the section centre of mass, its distance from both the force application point (i.e. the moment arm) and the cross-sectional location of interest, as well as the modal parameters of the considered mode(s). In this context, the translational mode shape, $\phi_{\boldsymbol{w,j}}$, is evaluated along the structure centre of mass, calculated for each section based on the geometry and density of the corresponding beam segment. The translational mode shape computed at both sides of the deck can be used to derive the corresponding rotational mode shape, $\phi_{\boldsymbol{\theta,j}}$, through geometrical considerations. It is important to emphasise that there is no specific threshold in $\phi_{\boldsymbol{\theta,j}}$ that can be used to classify a mode as mainly bending, mainly torsional, or a balanced combination of bending and torsion. In fact, the relevance of torsional effects depends not only on the relative amplitudes of translational and rotational components of the mode shape, but also on the associated modal masses and the loading moment arm, as will be further discussed in Section 5. Nevertheless, the proposed framework is general and can therefore be applied to estimate the vibration contribution of any vertical mode, including pure bending, pure torsional and bending-torsional coupled modes.

3. Serviceability experimental validation

This section presents and discusses the experimental tests conducted on the Bumerang Bridge (Norway) (Mo et al., 2019) to validate the proposed method for bending-torsion serviceability assessment. Section 3.1 describes the structural characteristics and testing setup, while Section 3.2 shows the comparison between experimentally recorded vibrations and those numerically predicted by applying the method to the specific test case.

(a) (b)

Figure 3. Bumerang footbridge in Oslo, Norway.

3.1. Structure description and test setup

Located in Oslo, the Bumerang bridge serves as a key link within the Groruddal area pedestrian and cycling network, connecting the city centre with eastern recreational areas (see Figure 3). The bridge is constructed from weathering steel, best known under the trademark COR-TEN steel, a rusty material which provides a durable, low-maintenance solution that is well-suited to the Norwegian climate. However, as a steel structure with slender design, it is relatively flexible, potentially prone to pedestrian-induced vibrations.

In line with this expectation, the bridge was selected based on preliminary dynamic tests, which revealed that the first vertical mode has: (a) a natural frequency within the typical range of pedestrian pacing frequencies, suggesting its sensitivity to human-induced vibrations, and (b) a mixed bending-torsional mode shape, making the structure particularly suitable for validating the proposed model. Torsional vibrations arise due to the structural asymmetry in plan, elevation, and cross-section, as detailed in the following.

Figure 4 presents the structure technical layout and typical cross-section, with structural characteristics described below. The plan view of the footbridge follows a curved, boomerang-like path to align with adjacent routes while avoiding trees and other natural obstacles in the surrounding forest. Supported between concrete abutments by three slender steel columns, the bridge has a total curved length of 83 m subdivided into four spans: two fully straight spans of 20.25 m, one span covering most of the curve with a curved length of 20.5 m, and a final span that ends the curve and continues straight which measures 22.5 m. The abutments are positioned with a 1.9-meter elevation difference, and the bridge deck presents a space-varying slope to accommodate this vertical offset. The structure is designed as a continuous steel box girder with a trapezoidal cross-section, positioned asymmetrically within the deck to counteract the torsional effects caused by the boomerang-shaped alignment. The girder cross-section maintains constant dimensions along the length of the footbridge, with a smaller base of 700 mm, a larger base of 900 mm, and a height of 850 mm. Cantilevered wings, acting as discrete stiffening elements, extend asymmetrically from the box girder, providing a standard 3-meter deck width which expands to 4 metres at the curve. A tapered reinforced concrete slab, with an average thickness of 100 mm, is placed atop, adapting in width to match the deck varying breadth. The concrete slab collaborates with the steel box girder by means of shear stud connectors.

The dynamic testing employed a traditional monitoring system with ten PCB 393B31 piezoelectric mono-directional accelerometers, operating at a sampling frequency of 100 Hz. Data acquisition was performed using a HBM system. To achieve broad spatial coverage of the structural response, accelerations were recorded at predefined locations along both sides of the structure, corresponding to the inner and outer curves (axis A and C in Figure 4, respectively). On the outer side, only vertical accelerations were measured, while on the inner side, both vertical and radial-horizontal components were acquired. This measurement arrangement was selected to match the expected dynamic behaviour of the system, in which sections translate and rotate with negligible transverse deformation, as discussed in more detail in Section 3.2.

Due to the limited number of available accelerometers, the full set of measurement locations and directions was obtained through a multi-setup testing approach. As illustrated in Figure 4, measurement points are marked with coloured markers: empty red circles indicate reference locations used across multiple setups, while filled blue circles denote positions instrumented in a single setup. To ensure measurement redundancy for consistent dataset alignment, each setup included at least four reference sensors (two measuring vertical accelerations and two measuring radial-horizontal accelerations) and a set of mobile sensors repositioned to progressively cover the remaining measurements.

Accelerations acquired under ambient environmental conditions served as input for Operational Modal Analysis (OMA), which was employed to identify the modal properties of the structure. Specifically, the COVariance-driven Stochastic Subspace Identification (SSI-COV) (Peeters & De Roeck, 1999) was employed. Following the PoSER (Post Separate Estimation Re-scaling) approach, modal parameters were estimated independently for each setup and subsequently re-scaled and merged to construct global mode shapes. Re-scaling was performed using a least-squares fitting procedure on the reference sensor portions of each

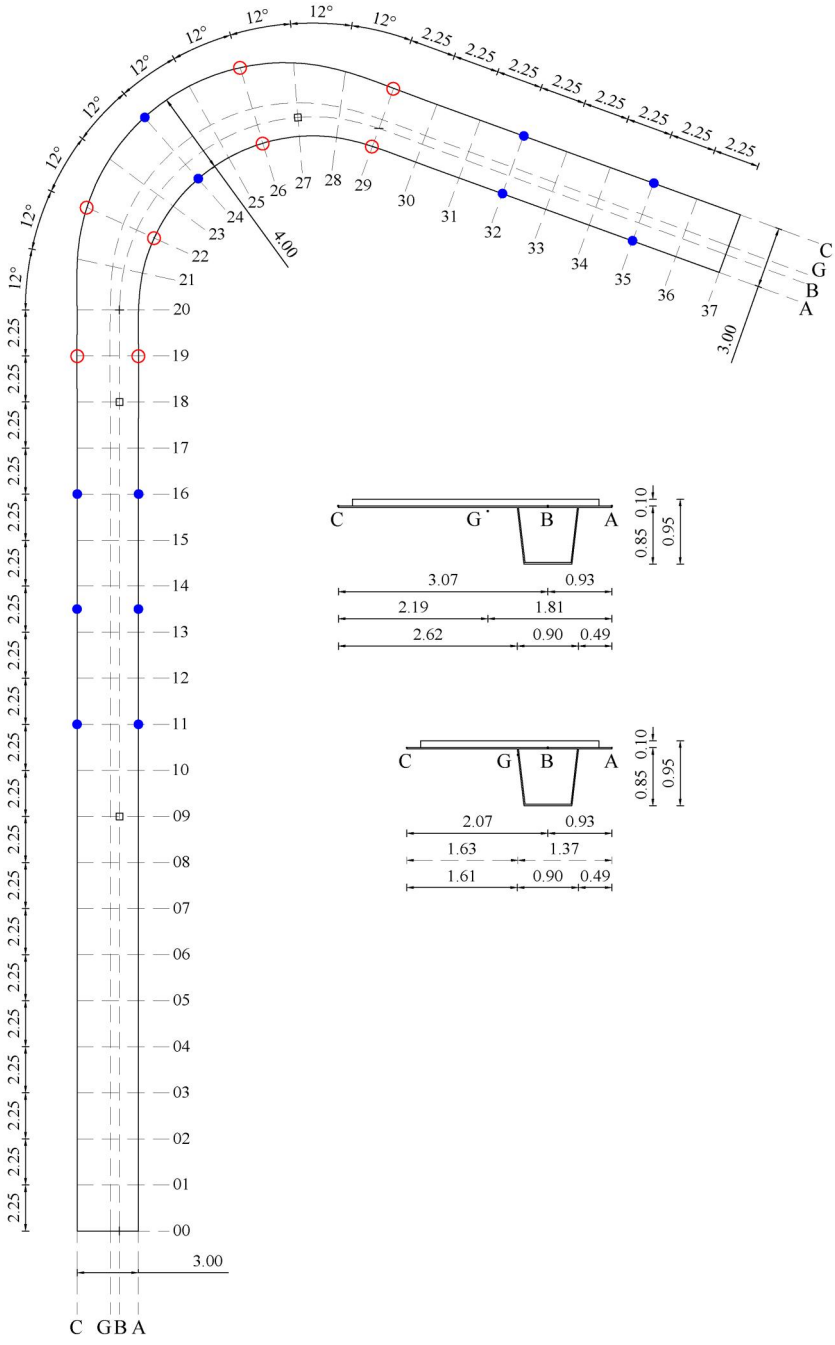

Figure 4. Bumerang bridge plan view and cross-sections with extreme widths (3 and 4 m), with accelerometer locations indicated by empty red circles (multi-setup reference sensors) and by filled blue circles (single-setup sensors).

partial mode shape, to ensure consistency across setups. This procedure revealed a first mode primarily characterised by horizontal motion, while the second, third, and fourth modes exhibited vertical bending-torsional behaviour. Modal frequencies and damping ratios were obtained as the average of the OMA results across all setups, leading to natural frequencies of 2.93, 3.38, 4.85, and 5.58 Hz (as reported in Table 2), and damping ratios of approximately 0.5% for all modes.

A Finite Element Model (FEM) of the structure was developed using Strand7, as illustrated in Figure 5. The model employs shell elements to represent the bridge deck box girder, with a layered shell formulation for the concrete slab. The columns are modelled using beam elements. In total, the FEM model consists of about 2200 nodes, 115 beam elements and 2700 plate elements. Nodes are spaced at an interval of 2.25 m along the straight segments, corresponding to the locations of the stiffening elements present in each section marked in Figure 4. The mesh is refined along the curved segment to ensure a more accurate

Table 2. Comparison between experimental and FEM-derived modal parameters corresponding to mode 1 (first horizontal mode), mode 2 (first vertical mode), mode 3 (second vertical mode), and mode 4 (third vertical mode).

	Mode 1	Mode 2	Mode 3	Mode 4
Experimental natural frequency (Hz)	2.93	3.38	4.85	5.58
Numerical natural frequency (Hz)	2.97	3.31	4.97	5.73
Natural frequency error (%)	1.37	2.07	2.47	2.69
Modal assurance criterion (-)	0.96	0.96	0.94	0.85

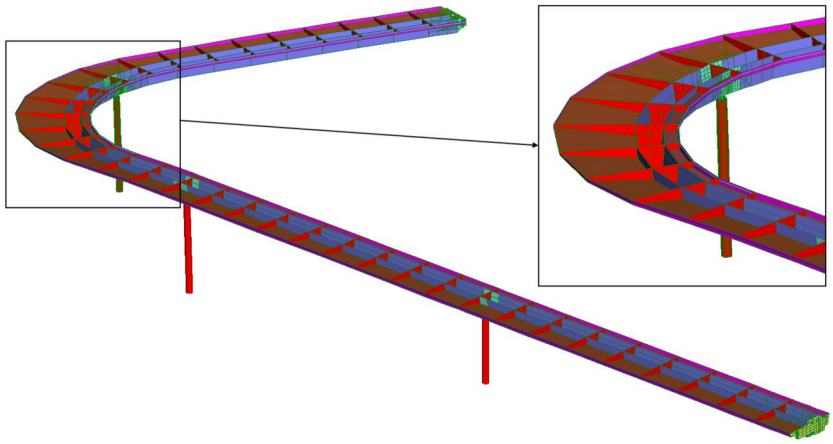

Figure 5. Finite element model of the Bumerang bridge in Strand7 with deck hidden; zoom on the curve highlights cross-section geometrical variation.

representation of the geometry and local modal behaviour. A similar refinement has been applied to the pier in the curved segment and at the abutments. In addition to the self-weight of the structural elements (which depends on the material density and area), the superimposed dead loads include the weight of the concrete slab, the waterproofing and surfacing layers, and the pedestrian railings. As boundary conditions, the FEM model considers the structure supported on top of the steel columns (fully fixed) and resting on the abutments, which provide only vertical restraint allowing rotations. The FEM was calibrated based on experimentally identified modal characteristics. A comparison between the experimental and calibrated FEM modal parameters is presented in Table 2 and Figure 6, indicating a good correlation in both natural frequencies and mode shapes, especially for the lower modes. In particular, the second mode, corresponding to the first vertical mode, is the primary focus for the vertical serviceability assessment addressed in this paper. In this regard, the FEM only purpose is to refine the spatial resolution of the second mode shape, as further explained in Section 3.2. This is helpful with the objective of this work, particularly in the context of parametric microscale pedestrian flow modelling (see Section 4.2). In practical serviceability applications, however, a detailed FEM is not required to apply the proposed method. For this reason, no further modelling details are provided.

In addition to environmental conditions, accelerations were also recorded under pedestrian loading. Three individuals, differing in gender, age, and weight, walked one at a time at about 1.34 m/s (pre-selected as widely recognised as the typical walking velocity under undisturbed conditions (Buchmueller & Weidmann, 2006)) along the outer side of the structure. Compared to walking along the centreline, this positioning amplifies the excitation of torsional vibrations. The maximum pedestrian-induced structural accelerations, experimentally recorded by sensors, are compared to numerical predictions computed in accordance with both Sections 2.1 and 2.2, to discuss the operation of the traditional pure bending framework and the bending-torsion coupled framework, respectively, in cases where eccentricity is present in both the structure and the loading. Details concerning the test-based numerical computations are provided below, beginning with the general bending-torsion formulation, followed by the analytical simplifications introduced by the traditional bending-based method.

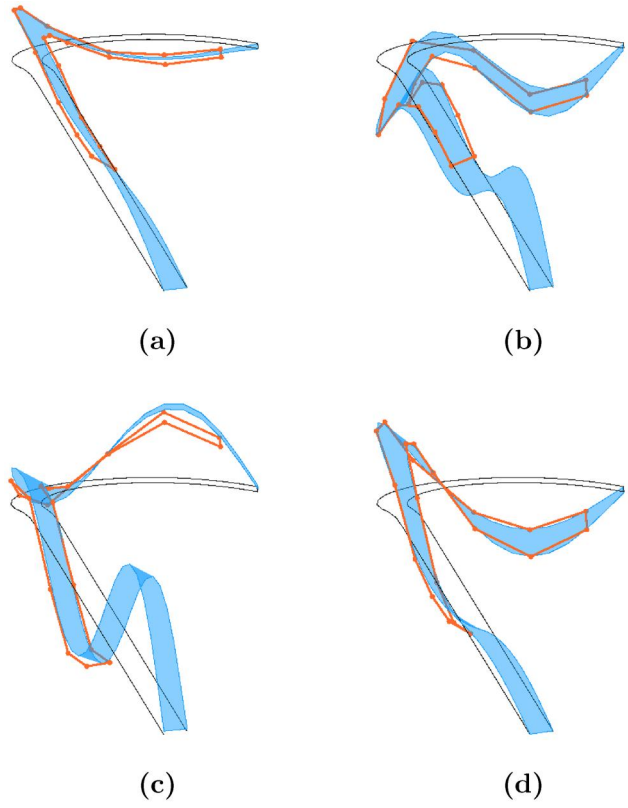

Figure 6. Bumerang bridge undeformed state in black, experimentally identified mode shapes in red (bold) and FEM mode shapes in blue, for the first (a), second (b), third (c), and fourth (d) modes.

3.2. Test-based numerical simulation and validation

The numerical analysis focuses on the acceleration contribution associated with the second mode ($j = 2$), the first to exhibit predominant vertical vibrations. The curved span (sections 18–27 in Figure 4) is selected for evaluations, as this is where the examined mode attains its maximum vertical amplitude. The considered span consists of sections with varying geometry, leading to shifts in the centre of mass

along its length. As shown in Figure 4, the distance between points A (the inner deck edge) and B (the centre of torsional stiffness, which also coincides with the centre of bending stiffness) remains constant, while the distance between B and C (the outer deck edge) increases along the curve. The mass associated with each section is evaluated based on the tributary area approach; therefore, since the spacing between consecutive sections varies, each section has a different mass, mass distribution, centre of mass, and corresponding moment of inertia. For instance, Figure 4 illustrates how geometric variation affects the centre of mass (G), using as examples two cross-sections with deck widths of 3 and 4 m. This procedure enables the assembly of the translational and rotational mass matrices, $\boldsymbol{M_w}$ and $\boldsymbol{M_\theta}$.

For each section, the degrees of freedom are defined as the vertical displacement w of the centre of mass G and the rotational angle θ, as depicted in Figure 7. Indeed, for the specific case study, the transverse deformation of the section is negligible: by linearising the FEM-derived deflections at the cross-sectional edges (A and C) to simulate the deflection of G, an error of approximately 1% compared to the FEM simulation is obtained. As a result, only two degrees of freedom are used, describing the rigid translational and rotational motion of the section, assuming that the cross-section remains transversely undeformed. Given the high Modal Assurance Criterion (MAC) values for the second mode shape (please refer to Table 2), the FEM-derived mode shape components are incorporated into the analysis, as they provide a more detailed spatial definition along the bridge compared to the experimentally obtained modes. The vertical components of the mode shape $\phi_{w,2}$ are computed using the FEM at the centre of mass G defined for each section. Additionally, the FEM-derived vertical components of the mode shape at the deck edges (outer points A and C) are used to determine the rotational mode shape $\phi_{\theta,2}$. Finally, the modal mass M_2^* is calculated by weighting the translational and rotational mass matrices, $\boldsymbol{M_w}$ and $\boldsymbol{M_\theta}$, by the corresponding mode shapes, $\phi_{w,2}$ and $\phi_{\theta,2}$ (see Equation (13)).

For each test subject, pedestrian loading is calculated using the step-by-step model by Li et al. (2010) (Equation (4)), considering individual weights of 50, 65, and 75 kg, along with a walking speed of 1.34 m/s. This velocity corresponds to a step frequency of 1.91 Hz, calculated using Equation (5), and a step length of 0.70 m, computed as the ratio of speed to step frequency. During the experimental campaign, pedestrians were required to walk as close as possible to the railing along the outer side of the deck C. This implies that their walking loading produces a moment with lever arm equal to the radial-horizontal distance from point C to the centre of mass G, which varies across each nodal section. To ensure that the modal force is amplified according to the mode shape amplitude at each foot position, the mode shapes and the moment arms are linearly interpolated at space intervals corresponding to the step length.

The modal equation of motion of Equation (12) is applied with the experimentally identified natural frequency and damping ratio. The derived modal amplitude is used to determine modal accelerations through Equation (16). Pure

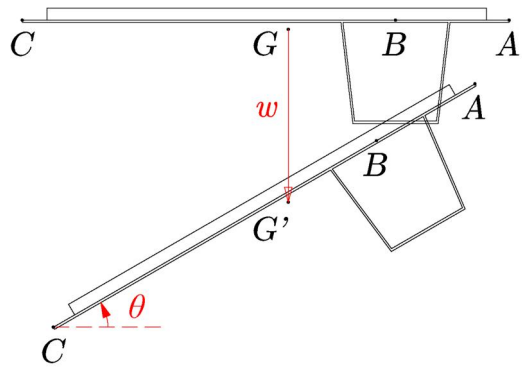

Figure 7. Cross-section rotational-translational motion characterised through two degrees of freedom, namely the vertical displacement w of the mass centre G and the angle θ.

translational and rotational accelerations are combined through Equation (17) to obtain the overall vertical acceleration at section 22, where the deflection is near its maximum and an accelerometer is installed for comparison. Within this section, the external edge C is selected, where the distance from the centre of mass G, denoted by e, is greatest, implying the highest rotational contribution to the vertical response. The maximum vertical acceleration over time, due to the combined effects of bending and torsion, is evaluated numerically for each test subject and compared with the maximum accelerations experimentally recorded at the outer edge of section 22, illustrated in Figure 8. This comparison, presented in Table 3, demonstrates the effectiveness of the proposed method, with a relative error $\delta_{\text{rel}}(\ddot{W}_C, \ddot{W}_C^{\text{exp}})$ between the experimental ($\ddot{W}_C^{\text{exp}}$) and numerical ($\ddot{W}_C$) structural maximum accelerations of approximatively 2% for the first two test subjects, and around 10% for the third. The greater error observed for the third subject is likely due to the subject walking at an unsteady speed, deviating from the target velocity of 1.34 m/s.

A similar simulation is conducted according to the traditional approach, which considers only the bending contribution to the vertical displacement, $\boldsymbol{w}$, as a single degree of freedom. This approach leads to Equation (1), which only considers the translational component of the modal mass and neglects pedestrian-induced moments in the modal force. With this simplification, the numerically obtained maximum accelerations ($\ddot{w}_C$), presented in Table 3, exhibit a relative error $\delta_{\text{rel}}(\ddot{w}_C, \ddot{W}_C^{\text{exp}})$ of over 50% compared to the experimental values ($\ddot{W}_C^{\text{exp}}$) for all three test subjects. Comparable outcomes are observed by comparing the experimental and numerical Root Mean Square (RMS) peak accelerations, with errors for the three test subjects amounting to 13.17, 24.28 and 21.22 % in the case of the bending-torsion framework, respectively, and significantly higher errors of 48.78, 44.03 and 64.56 % when using the traditional bending-only approach. These results underscore the importance of accounting for the combined effects of torsional and bending vibrations in cases involving asymmetric geometries, eccentric loads and torsional modes within the range of typical pedestrian pacing frequencies, as the vertical

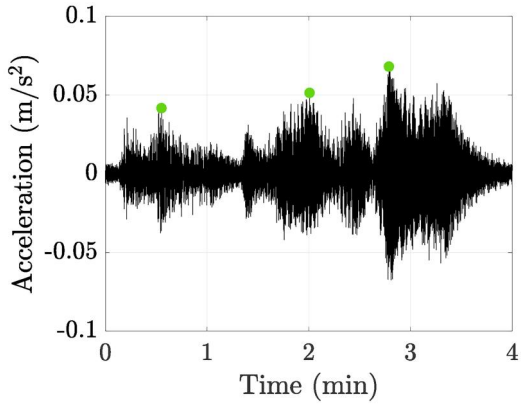

Figure 8. Experimentally measured accelerations induced by the three test subjects, with corresponding peak values indicated by green dots.

Table 3. Maximum accelerations for each test subject (50, 65, and 75 kg) evaluated both experimentally ($\ddot{W}_C^{exp}$) and numerically, considering the combined flexural and torsional vibration contributions ($\ddot{W}_C$) and the flexural vibration contribution only ($\ddot{w}_C$), with corresponding relative errors (δ_{rel}).

Test subject #	1	2	3
$\ddot{W}_C^{exp}$ (m/s^2)	0.0417	0.0514	0.0681
$\ddot{W}_C$ (m/s^2)	0.0406	0.0528	0.0609
$\delta_{rel}(\ddot{W}_C, \ddot{W}_C^{exp})$ (%)	2.64	2.72	10.57
$\ddot{w}_C = \ddot{w}_G$ (m/s^2)	0.0183	0.0238	0.0274
$\delta_{rel}(\ddot{w}_C, \ddot{W}_C^{exp})$ (%)	56.12	53.70	59.77

contribution induced by torsional rotations is significant and cannot be neglected.

4. Parametric numerical simulations

This section presents extended numerical simulations conducted to assess the influence of torsional effects on structural vibrations induced by pedestrian excitation, by systematically varying pedestrian loading configurations. Specifically, Section 4.1 investigates the impact of varying the position of individual pedestrians relative to the structure centre of mass, which results in different moment arms, and Section 4.2 addresses the effect of different traffic densities in crowd scenarios, which lead to diverse load distributions on the deck.

4.1. Effect of offset in single pedestrian trajectories

To generalise the findings presented in Section 3.2, numerical analyses are conducted considering a 65 kg pedestrian walking along trajectories with different offsets from the structure axis of mass centres. These simulations involve the same dynamic loading but differ in moment arm d, and consequently in the magnitude of the pedestrian-induced moment in the modal generalised force (see Equation (15)). Additionally, the structural vertical acceleration is calculated at different positions on the section through Equation (17), with each position having varying eccentricities e. Both the moment arm d and eccentricity e vary within the range from $+2.19$ m at C (outer side) to -1.81 m at A (inner side).

Figure 9(a) illustrates the numerically obtained accelerations along the z-axis as a function of the moment arm d of the pedestrian loading (x-axis) and the geometrical eccentricity e (y-axis), enabling an analysis that accounts for both loading and structural eccentricities relative to G (corresponding to zero on both x and y axes). Accelerations are evaluated using both the traditional bending approach, represented by the transparent surface with a black edge, and the proposed bending-torsion framework, represented by the solid shaded surface. As expected, this comparison graphically demonstrates that the structural acceleration evaluated using the traditional pure-bending approach remains constant, irrespective of the pedestrian and structural positions. In contrast, the proposed method accounts for both variables, leading to results that vary depending on the combination of d and e.

Figure 9(b) illustrates the relative difference between the traditional framework and the proposed method, i.e. the discrepancy in structural response when torsional effects are excluded versus included. The traditional assessment is limited to the case of a pedestrian walking perfectly along the structure axis of mass centres (with $d = 0$) inducing acceleration at the mass centre of the examined section ($e = 0$). Therefore, the maximum discrepancies occur when both d and e are at their maximum values and have the same sign. In such instances, relative differences can reach almost 250% (see Figure 9(b)). These analytical results further highlight the excessive simplicity of the traditional method in predicting human-induced vibrations, as the structural acceleration depends critically on both the position of the load and the location where the structural response is evaluated: the greater the eccentricity of the external forcing, the stronger the induced torsion, resulting in increased cross-sectional rotation and amplified vibrations at points farther from the centre of mass.

4.2. Effect of crowd flow density

To fully assess the dynamic behaviour of footbridges due to human excitation, it is essential to evaluate the impact of torsional effects not only from individual pedestrians but also from pedestrian crowds. While an individual walking along an eccentric trajectory with respect to the structure centre of mass generates a clearly defined torsional moment, the situation becomes more complex in the case of a crowd. In such scenarios, pedestrians may simultaneously occupy both sides of the deck, with opposing moment arms relative to the axis of mass centres. This distribution can lead to a reduction or partial compensation of the overall torsional effects, thereby reducing the total torsional contribution to the structural response.

To investigate the significance of torsional accelerations in vertical motion under crowd loading, numerical simulations are performed considering crowds of varying densities. These analyses aim to determine the extent to which torsional components influence the vertical dynamic response of the structure when subjected to realistically spatially distributed pedestrian loads. To this aim, crowd dynamics is

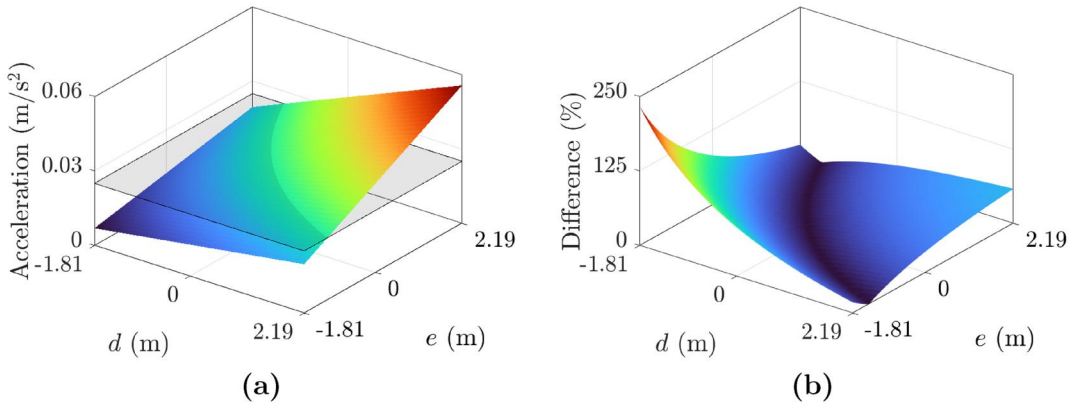

Figure 9. Vertical structure accelerations as a function of pedestrian moment arm d and response eccentricity e (where for both d and e, −1.81 corresponds to point *A*, 0 to *G*, 2.19 to *C*): (a) comparison between bending-only (black-edged transparent surface) and bending-torsion (filled shaded surface) models; (b) relative difference between the two.

simulated using the Social Force Model (SFM), a widely adopted approach that represents pedestrian movement as the result of social, psychological, and physical interaction forces (Helbing et al., 2005). Specifically, the SFM models each pedestrian individually in a microscopic framework, where trajectories and velocities are updated at each time step based on the surrounding environment. Each pedestrian is assigned a specific desired walking speed, representing the speed they would maintain in the absence of external influences. Their motion is governed by a combination of forces, including attractive forces towards a destination, social attraction to visual stimuli or sub-group members, repulsive interactions with other pedestrians, and avoidance of obstacles or boundaries.

The method originates from Helbing and Molnár (1995), and numerous adaptations of the SFM have since been proposed. In this study, the version of the SFM released by Bassoli and Vincenzi (2021) is adopted, calibrated according to the Weidmann's speed-density relationship (Weidmann, 1993). The latter provides an empirical formulation for average pedestrian velocity under free-to-congested conditions; accordingly, tuning the SFM to reproduce it supports a realistic simulation of crowd dynamics across varying traffic levels. Pedestrian densities ranging from 0.2 to 1.5 ped/m^2 (at 0.1 ped/m^2 increments) are investigated by setting the corresponding number of individuals on the deck as input to the SFM. Specifically, crowd density is maintained constant throughout the simulation by reintroducing each pedestrian onto the structure after they exit, ensuring a steady number of individuals on the deck at all times. The detailed procedure is described in Eslami Varzaneh et al. (2024) and summarised in the following:

- For each density level, 150 independent simulations are conducted to ensure statistical robustness of the results, each initialised with randomised starting conditions. These include randomly assigned pedestrian initial positions and desired walking speeds, drawn from a normal distribution of free-flow walking velocities (Buchmueller & Weidmann, 2006), with a mean of 1.34 m/s and a standard deviation of 0.26 m/s. Additionally, pedestrian body weights are randomly assigned based on a log-normal distribution, reflecting typical population statistics (Portier et al., 2007), with a mean of 73.85 kg and a standard deviation of 15.68 kg.
- The SFM provides the time-varying position and velocity of each pedestrian in the crowd, accounting for their interactions throughout the simulation. For instance, the trajectory followed by an example pedestrian within a simulated crowd flow is represented in Figure 10(a) (red line). Note that the just mentioned path exhibits irregularities, reflecting changes in the pedestrian desired direction and speed due to interactions with the surroundings. SFM outputs are then converted into dynamic loading, as detailed in the following. For each pedestrian, the two-dimensional velocity components obtained from the SFM simulation are combined to derive the instantaneous walking speed, from which the time-varying step frequency is computed through Equation (5), according to Bruno and Venuti (2008). The timing of each footstep is determined iteratively, with each step duration calculated based on the pacing frequency derived at the instant of the preceding footstep. The spatial position of each step is taken from the pedestrian two-dimensional trajectory generated by the SFM at the corresponding step application time. For the example pedestrian of Figure 10(a), this leads to the definition of the foot standing points marked by red circles.
- The force associated with each footfall is described via Equation (4) in line with Li et al. (2010). The overall walking-induced load from a single pedestrian is obtained by summing the contributions from all individual footfalls along their path. When applied to the pedestrian example in Figure 10(a), this results in the force depicted in Figure 10(b). While an isolated pedestrian is described by a periodic walking force (see Figure 1), a pedestrian within a crowd displays irregular gait patterns, with steps that vary from one another, as shown in Figure 10(b). To compute the total crowd-induced load, the forces generated by all pedestrians are superposed. This superposition is justified as the pedestrian flows generated by the SFM produce realistic temporal and

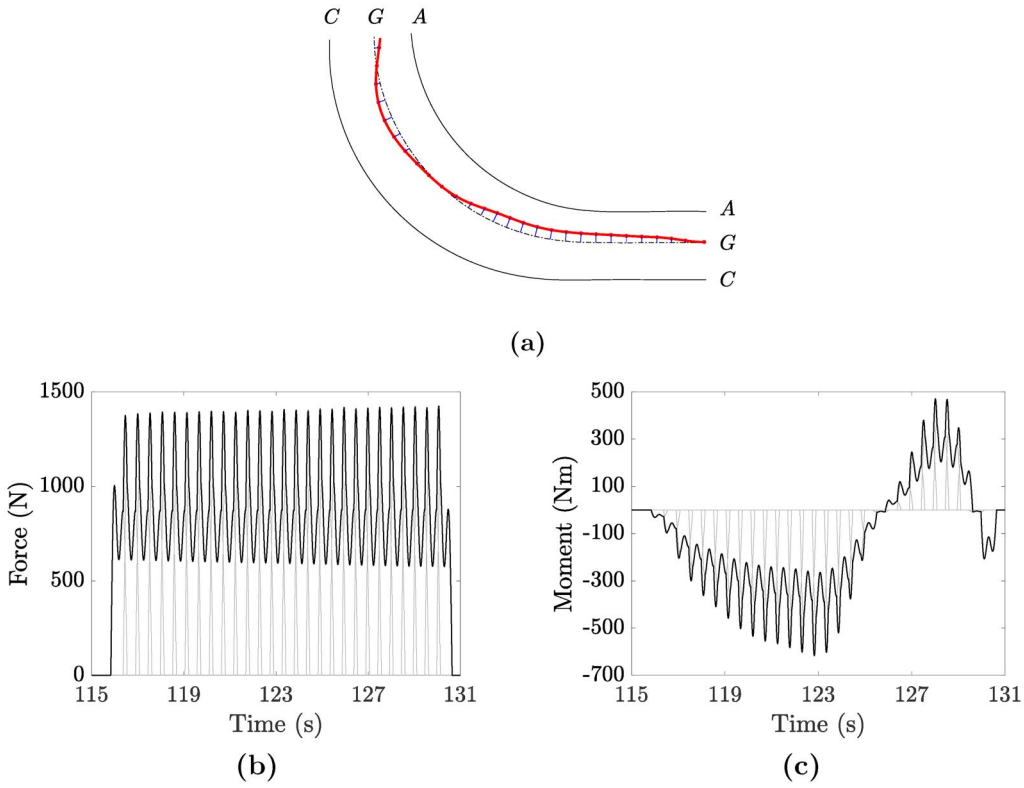

Figure 10. Single pedestrian walking within a SFM-simulated crowd: (a) path travelled to cross the examined span (bold red line), foot standing points (red markers) and corresponding moment arms (blue lines); (b) single step forces (grey) and overall force (black); (c) single step moments (grey) and overall moment (black).

spatial distributions of step forces: inter-subject variability is captured through the random assignment of desired walking speeds, while intra-personal variability emerges from the continuous adaptation of each pedestrian pace in response to external factors, including human-human interactions.

- The two-dimensional footstep coordinates generated by the SFM (e.g. red markers in Figure 10(a)) play a key role in evaluating the moment associated with each step force, as they enable the computation of the corresponding step moment arms (blue lines in Figure 10(a)). Accordingly, step forces (grey lines in Figure 10(b)) are multiplied by their respective moment arms to compute the step moments (grey lines in Figure 10(c)). The sign of each step moment depends on whether the foot placement is to one side or the other of the structure centre of mass (dash-dotted in Figure 10(a)). To calculate the total moment induced by the crowd, the step forces of all pedestrians are combined over time and space.
- To evaluate the overall crowd-induced modal generalised force for the bending-torsion combined framework, Equation (15) is used. Each step force is weighted by the translational mode shape amplitude evaluated at the footstep position, projected onto the axis of mass centres along its normal. Similarly, each step moment is scaled by the rotational mode shape amplitude at the footfall location. When the traditional bending-only framework is applied, the generalised modal force defined in Equation (15) simplifies accordingly, and the modal mass in Equation (13) reduces to include only the translational contribution. In this context, the influence of human-structure interaction could be captured by considering the equivalent modal parameters of the crowd-structure system instead of those of the empty footbridge (as suggested, for instance, by Bassoli, Van Nimmen, et al. (2018)). This aspect is worth noting but remains beyond the scope of the present work.

Crowd-induced structural accelerations predicted by the two approaches are shown in Figure 11, along with their relative difference. Blue indicates results from the traditional bending-only framework, red represents those from the proposed bending-torsion coupled approach, and black shows their discrepancy. Solid lines denote the mean maximum response from the 150 SFM simulations performed at each crowd density level, with standard deviation bands denoting the corresponding variability ranges. Particular attention is drawn to the trend of average maximum structural acceleration as a function of pedestrian density. Notably, this trend is not monotonically increasing in Figure 11(a): regardless of the method used (i.e. for both red and blue colours), acceleration levels rise with density up to a certain point, beyond which they slightly decrease. This observation underscores that increasing crowd density does not necessarily correspond to the most critical loading condition for the structure. On one hand, higher densities lead to greater total pedestrian mass, which typically amplifies structural response. On the other hand, congestion effects in denser crowds tend to reduce the average pedestrian step frequency. Depending on whether this frequency shift moves

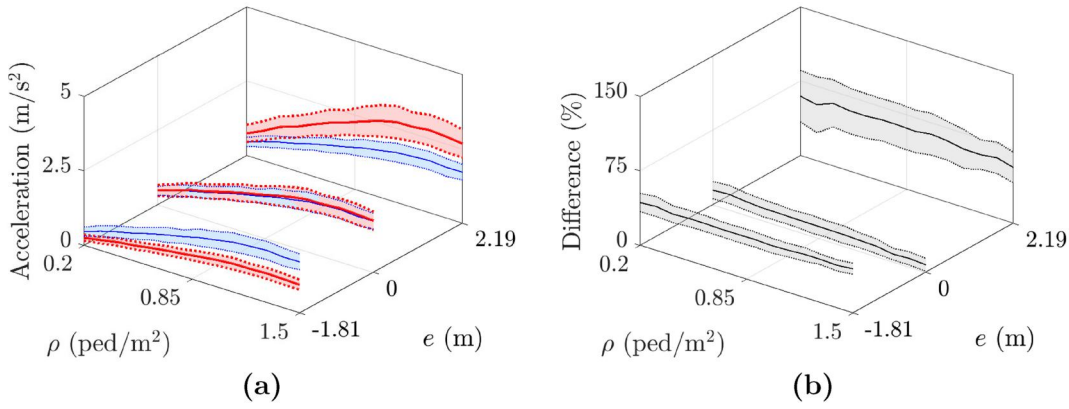

Figure 11. Vertical structural accelerations due to SFM-simulated crowds as a function of pedestrian density and response eccentricity e (where $e = -1.81$ at A, $e = 0$ at G, $e = 2.19$ at C), with solid lines showing the mean over 150 simulations and shaded areas denoting one standard deviation: (a) traditional bending-only approach (blue) and proposed bending-torsion coupled framework (bold red); (c) relative difference between the two (black).

closer to or farther from the structure natural frequency, the dynamic amplification may increase or decrease. Therefore, the worst-case scenario depends on the interplay between mass loading and frequency alignment, and understanding this interaction is essential for identifying the most demanding crowd configuration for a given structure.

The results obtained using the two methods present a key difference. The traditional approach does not account for torsional rotations and therefore predicts identical accelerations at all points across the cross-section, regardless of their eccentricity e. In contrast, the proposed method combines bending and torsional contributions to the vertical acceleration. These contributions are additive and amplify the response at point C (and more generally where $e > 0$), while they are opposing and thus partially cancel out at point A ($e < 0$). As expected, the traditional method underestimates the accelerations at point C compared to those predicted by the proposed method, and overestimates them at point A. At the mass centre G ($e = 0$), the accelerations predicted by the two methods still do not coincide, as the associated modal mass differs between the two frameworks. All this is graphically evident in Figure 11(a) and quantitatively supported by Tables 4–6, which report the mean maximum structural accelerations at points G, C, and A, respectively, evaluated using the bending-torsion ($\ddot{W}_G$, $\ddot{W}_C$, $\ddot{W}_A$) and traditional bending-only ($\ddot{w}_G$, $\ddot{w}_C$, $\ddot{w}_A$) methods across varying crowd density levels.

Another noteworthy observation concerns the relative difference between the two modelling approaches. The average difference (black line in Figure 11(b)) is strongly influenced by the location along the cross-section at which structural acceleration is evaluated, while it remains nearly constant across different crowd densities. However, the variability (or dispersion, illustrated as the standard deviation band in Figure 11(b)) of this difference depends on the crowd density. As the crowd becomes denser, pedestrian distribution across the deck becomes more uniform, and the overall torsional contribution decreases. This is because pedestrians walking on opposite sides of the mass centre generate torsional actions of opposite sign, which tend to balance each other out, thereby reducing their combined influence on the structural response. Nevertheless, the relative difference between the two approaches does not vanish along the mass centre G ($e = 0$), even at high crowd densities. This is due to the fact that, although the crowd may be symmetrically distributed with respect to the deck geometrical centreline (i.e. midpoint between edges A and C), this centreline does not coincide with the mass centre G, which is offset due to the structural eccentricity of the cross-section.

5. Multiplication factors for simplified assessment

To enable a simplified assessment, multiplication factors are analytically derived, allowing adjustment of accelerations obtained by considering bending effects only. This strategy retains the practicality of the traditional bending-only framework while extending it through straightforward correction terms that account for torsional rotation induced by human loading at multiple cross-sectional positions. Two multiplication factors are introduced: the first, α_{tors}, adjusts the vertical acceleration predicted at the cross-sectional centre of mass G to incorporate torsional contributions; the second, $\alpha_{\text{pos}}(H)$ scales this value to estimate the acceleration at any point H across the section, capturing the increasing influence of rotational effects with distance from G. For these reasons, they are respectively referred to as the torsional multiplication factor and the positional multiplication factor, as indicated in their respective subscripts.

The torsional multiplication factor α_{tors} is derived by mathematically comparing the modal displacement computed through the bending-only ($\phi_{w,j}\ q_j$) and bending-torsion ($\phi_{w,j}\ Q_j + \phi_{\theta,j}\ Q_j$) frameworks. When a consistent normalisation of the modes is adopted, this equals comparing the modal forces from the two frameworks. This requires $\phi_{w,j}$ to be the same within the two frameworks, meaning that the maximum vertical displacement component is normalised to unit and rotational components are scaled accordingly. Note that this would not be valid if the modes were normalised to modal masses. Under these conditions, the multiplication factor α_{tors} is estimated by dividing the modal generalised force (right-hand side) of the Equations (12) and (3), leading to the following expression:

Table 4. Mean maximum structural acceleration at point G for different crowd densities, comparing evaluations from the bending-only ($\ddot{w}_G$) and combined bending-torsion ($\ddot{W}_G$) approaches, simplified predictions using the torsional multiplication factor (α_{tors}) and corresponding relative difference (δ_{rel}).

Torsional factor α_{tors} (-)	0.9727			
Density (ped/m^2)	0.30	0.70	1.10	1.50
$\ddot{W}_G$ (m/s^2)	0.6562	1.2813	1.7498	1.7321
$\ddot{w}_G$ (m/s^2)	0.6535	1.2252	1.6789	1.7168
$\ddot{w}_G\alpha_{\text{tors}}$ (m/s^2)	0.6357	1.1918	1.6331	1.6699
$\delta_{\text{rel}}(\ddot{w}_G\alpha_{\text{tors}}, \ddot{W}_G)$ (%)	3.1302	6.9845	6.6699	3.5861

Table 5. Mean maximum structural acceleration at point C for different crowd densities, comparing evaluations from the bending-only ($\ddot{w}_C$) and combined bending-torsion ($\ddot{W}_C$) approaches, simplified predictions using the positional multiplication factor ($\alpha_{\text{pos}}(C)$) alone or in combination with the torsional multiplication factor (α_{tors}) and corresponding relative differences (δ_{rel}).

Positional factor $\alpha_{\text{pos}}(C)$ (-)	1.5443			
Density (ped/m^2)	0.30	0.70	1.10	1.50
$\ddot{W}_C$ (m/s^2)	0.3596	0.7021	0.9588	0.9491
$\ddot{w}_C = \ddot{w}_G$ (m/s^2)	0.6535	1.2252	1.6789	1.7168
$\ddot{w}_G\alpha_{\text{tors}}\alpha_{\text{pos}}(C)$ (m/s^2)	0.3483	0.6530	0.8948	0.9150
$\delta_{\text{rel}}(\ddot{w}_G\alpha_{\text{tors}}\alpha_{\text{pos}}(C), \ddot{W}_C)$ (%)	3.1302	6.9845	6.6699	3.5861
$\ddot{W}_G\alpha_{\text{pos}}(C)$ (m/s^2)	0.3596	0.7021	0.9588	0.9491
$\delta_{\text{rel}}(\ddot{W}_G\alpha_{\text{pos}}(C), \ddot{W}_C)$ (%)	0.0000	0.0000	0.0000	0.0000

Table 6. Mean maximum structural acceleration at point A for different crowd densities, comparing evaluations from the bending-only ($\ddot{w}_A$) and combined bending-torsion ($\ddot{W}_A$) approaches, simplified predictions using the positional multiplication factor ($\alpha_{\text{pos}}(A)$) alone or in combination with the torsional multiplication factor (α_{tors}) and corresponding relative differences (δ_{rel}).

Positional factor $\alpha_{\text{pos}}(A)$ (-)	0.5479			
Density (ped/m^2)	0.30	0.70	1.10	1.50
$\ddot{W}_A$ (m/s^2)	1.0134	1.9787	2.7022	2.6748
$\ddot{w}_A = \ddot{w}_G$ (m/s^2)	0.6535	1.2252	1.6789	1.7168
$\ddot{w}_G\alpha_{\text{tors}}\alpha_{\text{pos}}(A)$ (m/s^2)	0.9817	1.8405	2.5220	2.5789
$\delta_{\text{rel}}(\ddot{w}_G\alpha_{\text{tors}}\alpha_{\text{pos}}(A), \ddot{W}_A)$ (%)	3.1302	6.9845	6.6699	3.5861
$\ddot{W}_G\alpha_{\text{pos}}(A)$ (m/s^2)	1.0134	1.9787	2.7022	2.6748
$\delta_{\text{rel}}(\ddot{W}_G\alpha_{\text{pos}}(A), \ddot{W}_A)$ (%)	0.0000	0.0000	0.0000	0.0000

$$\alpha_{\text{tors}} = \left(1 + \frac{\phi_{\theta,j,z}}{\phi_{w,j,z}} d\right) \Big/ \left(1 + \frac{\phi_{\boldsymbol{\theta},j}{}^{\mathrm{T}} \boldsymbol{M}_{\boldsymbol{\theta}} \phi_{\boldsymbol{\theta},j}}{\phi_{\boldsymbol{w},j}{}^{\mathrm{T}} \boldsymbol{M}_{\boldsymbol{w}} \phi_{\boldsymbol{w},j}}\right) \tag{18}$$

with subscript z indicating the nodal section of interest.

This factor allows for the inclusion of the rotational modal mass (in the denominator) and the torsional contribution in the modal action (in the numerator), weighted by the rotational mode shape and amplified by the moment arm d. The definition of d is straightforward when simulating individual pedestrians, as it directly corresponds to the eccentricity of the pedestrian trajectory relative to the centre of mass. However, for crowds, d should be interpreted as an equivalent moment arm. For instance, assuming a uniform distribution of pedestrians along the deck, d can be estimated by calculating the offset between the centreline and the centre of mass, representing the resulting moment arm considering the balancing effects of people walking on opposite sides of the structure.

The positional multiplication factor $\alpha_{\text{pos}}(H)$ is derived from Equation (17) by comparing two cases: the structural response at a generic eccentric point H on the cross-section (characterised by an eccentricity e) and the response at the centre of mass G, where the eccentricity is zero and, consequently, the rotational contribution vanishes. By dividing the expressions for these two conditions, the positional multiplication factor is obtained as:

$$\alpha_{\text{pos}}(H) = 1 + \frac{\phi_{\theta,j,z}}{\phi_{w,j,z}} e \tag{19}$$

This factor accounts for the alteration in structural vertical acceleration, velocity, or displacement resulting from the rotational motion of the cross-section. The rotational contribution adds to (or subtracts from) the translational response in proportion to the eccentricity e, i.e. the distance between the generic point H and the centre of mass G.

The multiplication factors provide an a-priori estimation of the torsional contribution entity compared to bending-only vibrations at different cross-sectional locations. Indeed, by just knowing the modal parameters (masses and mode shapes) and the pedestrian offset to the structural centre of mass G (i.e. d), the torsional multiplication factor α_{tors} enables to quantify the contribution of torsion to the bending-torsion vibration coupling at G. Specifically, α_{tors} is around 1 when the torsional contribution is negligible, which occurs when the load is applied close to G or under symmetric crowd loading conditions around G. The positional multiplication factor $\alpha_{\text{pos}}(H)$ allows the estimation of the torsional rotation contribution to the response at the section outermost points (i.e. those farthest from G), based solely on the mode shapes and the distance e between the considered point H and G. Specifically, factor $\alpha_{\text{pos}}(H)$ is greater than 1 when the moment-induced rotation increases the vertical displacement caused by the force, and less than 1 otherwise.

To validate the proposed multiplication factors, the extended numerical simulations performed with both the bending-only and bending-torsion frameworks are employed for both single pedestrian and crowd loading scenarios, previously introduced in Sections 4.1 and 4.2, respectively. In the case of individual pedestrians, the structural accelerations computed at the centre of mass using the bending-only approach (see the black-edged surface of Figure 9(a) at structural point G, i.e. corresponding to $e = 0$) are multiplied by the torsional multiplication factor α_{tors}, and these estimates are compared against the values obtained using the full bending-torsion model (see the shaded surface of Figure 9(a) at $e = 0$). Additionally, the bending-only accelerations at the centre of mass are further scaled using the positional multiplication factor $\alpha_{\text{pos}}(H)$ to estimate structural accelerations at generic points H on the cross-section. These results are then compared to the bending-torsion outcomes computed directly at those locations (see Figure 9(a) for non-zero values of e). In both cases, the difference between full computations and simplified estimations turns zero due to the way α_{tors} and $\alpha_{\text{pos}}(H)$ have been defined, demonstrating the effectiveness of the multiplication factors in replicating the full bending-torsion response based on simplified bending-only results, regardless of the pedestrian trajectory (i.e. independently of d).

The same validation procedure is applied to crowd loading scenarios, with simulations performed at different pedestrian densities. For each density level, structural accelerations at

the centre of mass $\ddot{w}_G$ obtained from the bending-only model (see blue curve at $e = 0$ in Figure 11(a)) are corrected using the torsional multiplication factor α_{tors} and compared against those from the bending-torsion model $\ddot{W}_G$ (red curve at $e = 0$). Results for selected densities are presented in Table 4, with similar trends observed at other traffic levels.

These corrected accelerations $\ddot{w}_G\alpha_{\text{tors}}$ are then further scaled by the positional multiplication factor $\alpha_{\text{pos}}(H)$ to estimate accelerations at eccentric locations on the cross-section (e.g. $H = C$ and $H = A$). These estimates are compared with direct bending-torsion model outputs at the same locations (red curves at A and C in Figure 11(a)), as shown in Tables 5 and 6. In these tables, the relative difference δ_{rel} is calculated between the accelerations obtained using the bending-torsion method and those estimated by scaling the results from the bending-only framework.

The level of discrepancy remains consistent across all the locations on the section: in G ($\delta_{\text{rel}}(\ddot{w}_G\alpha_{\text{tors}}, \ddot{W}_G)$), in C ($\delta_{\text{rel}}(\ddot{w}_G\alpha_{\text{tors}}\alpha_{\text{pos}}(C), \ddot{W}_C)$) and in A ($\delta_{\text{rel}}(\ddot{w}_G\alpha_{\text{tors}}\alpha_{\text{pos}}(A), \ddot{W}_A)$). This indicates that differences stem primarily from the torsional multiplication factor, while the positional multiplication factor introduces no additional deviation. This is further confirmed by scaling $\ddot{W}_G$ from the bending-torsion model with the positional multiplication factor: $\delta_{\text{rel}}(\ddot{W}_G\alpha_{\text{pos}}(C), \ddot{W}_C) = 0$ and $\delta_{\text{rel}}(\ddot{W}_G\alpha_{\text{pos}}(A), \ddot{W}_A) = 0$, as reported in Tables 5 and 6.

Overall, under crowd conditions, the positional scaling maintains high accuracy, while the torsional correction introduces a moderate average deviation of about 6% across all densities. This discrepancy is primarily attributed to the non-uniform width of the footbridge along its length, which causes the equivalent moment arm d to vary spatially. Additionally, while the crowd centre of mass may, on average, be centred on the deck over the course of the simulation (as verified by averaging all step moment arms within each simulation), it can be eccentric at the specific time when the peak modal acceleration occurs, making the estimation of the equivalent moment arm d more challenging under crowd conditions. Nevertheless, the observed deviation is considered fully acceptable in view of the simplifications adopted. In conclusion, the two multiplication factors are analytically derived rather than empirically calibrated, ensuring exact results when no additional assumptions are required (i.e. for simulating single pedestrians). In crowd scenarios, however, the estimation of an equivalent overall moment arm introduces some approximation, as it relies on the assumption of a uniform spatial distribution of pedestrians in the crowd. While this may lead to slight deviations, the resulting differences remain limited and fully acceptable for practical applications.

Also, it is worth highlighting that, in the specific application case, the torsional multiplication factor α_{tors} results in a value slightly below unity, approximately 0.97 (see Table 4). This outcome can be explained by analysing the relative contributions of the torsional and vertical components in both the numerator and the denominator constituting the α_{tors} definition (see Equation (18)). Specifically, while the torsional rotation adds a small increment to the generalised force (through the crowd equivalent moment arm d, computed in line with the uniform distribution assumption, and the ratio $\phi_{\theta,j}/\phi_{w,j}$), the corresponding increase in modal mass is proportionally larger. In fact, the torsional modal mass represents about 7.5% of the vertical one, which leads to a greater increase in inertia than in forcing. As a result, the torsional effects (although aligned in direction with the vertical motion) contribute more to the system resistance than to its excitation, ultimately reducing the modal response compared to the vertical-only case.

For instance, if the crowd were not uniformly distributed but instead eccentric (e.g. due to a temporary concentration of pedestrians on one side of the deck), the value of the numerator could exceed that of the denominator due to the increased moment arm d. Similarly, even a limited load eccentricity d could lead to $\alpha_{\text{tors}} > 1$ when combined with either a relatively small torsional modal mass (i.e. reduced structural inertia to torsion) or a high ratio between the torsional and vertical mode shape amplitudes (i.e. stronger torsional contribution in the mode shape). In such cases, the torsional effects become non-negligible. On the other hand, regarding $\alpha_{\text{pos}}(H)$ (see Equation (19)), its value being greater or less than one depends on the ratio of rotational-to-translational mode shapes, as well as whether the torsional and bending contributions combine constructively (for example at C, where $e > 0$) or destructively (at A, where $e < 0$). This opposite behaviour is clear in Tables 5 and 6, respectively showing $\alpha_{\text{pos}}(C) > 1$ and $\alpha_{\text{pos}}(A) < 1$.

In conclusion, all this highlights how both multiplication factors (α_{tors} and $\alpha_{\text{pos}}(H)$) depend on the balance between the torsional action introduced by the loading and the structural torsional resistance. These factors can be calculated a-priori and may serve as useful indicators for determining whether more detailed investigations into torsional human-induced effects are necessary. In such cases, the traditional bending-only framework may still be adopted, as long as appropriate response amplification or reduction is applied to reflect torsional effects.

6. Conclusions

This study addresses a critical gap in the evaluation of pedestrian-induced dynamic effects on footbridges, particularly with regard to torsional vibrations. While traditional serviceability assessments primarily focus on vertical bending vibrations, this approach overlooks the significant influence of torsional effects, especially in footbridges with asymmetrical geometries and/or load distribution asymmetries which may activate torsional modes. The results presented in this paper emphasise the need for a more complete consideration of both bending and torsional dynamics in the analysis of pedestrian-induced vibrations.

The generalised model proposed here, which accounts for the coupling of bending and torsional vibrations, was validated through a detailed experimental test on a boomerang-shaped footbridge with an asymmetrical cross-section. This test involved pedestrians with varying weights walking along the outer side of the deck, to demonstrate the amplifying effect of eccentric loading on vertical vibrations. The

comparison between experimental and numerical results showed that the designed method effectively captures the combined bending and torsional responses, confirming the model accuracy and applicability.

Further numerical simulations considering varying eccentricities in pedestrian loading reinforced these conclusions. The increased vibrations observed with more eccentric load positions, particularly at points farther from the centre of mass, underline the inadequacy of conventional models in predicting real-world conditions. These results suggest that pedestrian-induced vibrations should be evaluated using a combined bending-torsion framework to ensure accurate predictions of structural behaviour and serviceability.

Similar conclusions can be drawn from the crowd simulations, even though torsional contributions may appear less significant due to the natural balancing effect caused by people walking on opposite sides of the deck. This balancing becomes more pronounced as the crowd density increases and the pedestrian distribution becomes more uniform. However, even when the external loading is symmetric, structural eccentricities can still lead to amplified accelerations at positions farther from the centre of mass. In addition, non-uniform pedestrian flows (for example, due to a temporary obstacle on one side of the deck) may increase torsional vibrations with growing crowd density. This suggests the need for further numerical investigations in future applications involving non-uniformly distributed crowds. These considerations underline the importance of adopting a bending-torsion framework not only for isolated pedestrians but also for dense pedestrian flows.

To retain simplicity in the assessment phase, two multiplication factors are proposed, enabling the extension of traditional bending-only evaluations to include torsional effects in a straightforward yet reliable manner, without the need for complex coupled simulations. The first multiplication factor accounts for torsional contributions at the centre of mass, while the second extrapolates the response to other cross-sectional points based on their positional eccentricity. These factors can be calculated in advance and used to decide if a more detailed study of torsional effects from pedestrians is needed. If so, the generalised bending-torsion framework can be used, or the classical bending-only method can be kept, with the response simply adjusted using these two factors to account for torsional effects.

Both the detailed and simplified methods proposed here are tested and validated against both single pedestrians and crowds, modelled accounting for inter-pedestrian variability, intra-personal variability due to external factors and human-human interactions. Furthermore, both the methods allow accounting for the main effects of human-structure interaction, namely the modal change in the system mass and damping. This can be achieved, for instance, by implementing the equivalent modal parameters of the crowd-structure system rather than those of the empty structure.

In conclusion, this study offers a more accurate and robust method for analysing footbridge dynamics under pedestrian loading. The inclusion of torsional effects is shown to be essential for capturing the true structural response, ensuring improved precision in serviceability checks and better protection of user comfort. Future developments should aim to extend the experimental validation to a broader range of bridge types, considering both single pedestrian and real crowd scenarios, to further confirm the general applicability and reliability of the proposed approach.

Indices and Counters

i	Footstep counter
j	Mode counter
k	Harmonic counter in Fourier series
m	Number of retained vibration modes
n	Number of discrete beam nodes

Structural Dynamics

$\boldsymbol{w}(t)$	Vertical displacement vector ($n \times 1$)
$\boldsymbol{\theta}(t)$	Torsional rotation vector ($n \times 1$)
$\boldsymbol{W}(t)$	Generalised displacement vector: $[\boldsymbol{w}(t); \boldsymbol{\theta}(t)]$ ($2n \times 1$)
$\boldsymbol{M_w}$	Translational mass matrix ($n \times n$)
$\boldsymbol{M_\theta}$	Rotational mass matrix ($n \times n$)
$\boldsymbol{M}$	Generalised mass matrix: $\mathrm{diag}(\boldsymbol{M_w}, \boldsymbol{M_\theta})$ ($2n \times 2n$)
$\boldsymbol{C_w}$	Translational damping matrix ($n \times n$)
$\boldsymbol{C_\theta}$	Rotational damping matrix ($n \times n$)
$\boldsymbol{C}$	Generalised damping matrix: $\mathrm{diag}(\boldsymbol{C_w}, \boldsymbol{C_\theta})$ ($2n \times 2n$)
$\boldsymbol{K_w}$	Translational stiffness matrix ($n \times n$)
$\boldsymbol{K_\theta}$	Rotational stiffness matrix ($n \times n$)
$\boldsymbol{K}$	Generalised stiffness matrix: $\mathrm{diag}(\boldsymbol{K_w}, \boldsymbol{K_\theta})$ ($2n \times 2n$)
$\boldsymbol{P_w}(t)$	Nodal pedestrian load vector ($n \times 1$)
$P_i(t)$	Footfall force from step i at its own spatial location and time t
$P(t)$	Sum of all step forces $P_i(t)$ evaluated at footfall locations (not nodal)
$\boldsymbol{d_\theta}$	Nodal moment arm vector for torsion ($n \times 1$)
d_i	Moment arm of the i-th footfall force
d	Global moment arm for force $P(t)$
$\boldsymbol{R}(t)$	Generalised nodal external load vector $[\boldsymbol{P_w}(t); \mathrm{diag}(\boldsymbol{P_w}(t))\boldsymbol{d_\theta}]$ ($2n \times 1$)
$\Phi_{\boldsymbol{w}}$	Mode shape matrix for displacements ($n \times m$)
$\Phi_{\boldsymbol{\theta}}$	Mode shape matrix for rotations ($n \times m$)
Φ	Mode shape matrix ($2n \times m$)
$\boldsymbol{q}(t)$	Modal amplitude vector ($m \times 1$)
$q_j(t)$	Modal amplitude of mode j
$\boldsymbol{Q}(t)$	Modal amplitude vector ($m \times 1$)
$Q_j(t)$	Modal amplitude of mode j
$\phi_{\boldsymbol{w,j}}$	Vertical mode shape vector for mode j ($n \times 1$)
$\phi_{\boldsymbol{\theta,j}}$	Rotational mode shape vector for mode j ($n \times 1$)
$\phi_{w,j,i}$	Vertical mode shape amplitude of mode j at the spatial location of step i
$\phi_{\theta,j,i}$	Rotational mode shape amplitude of mode j at the spatial location of step i
M_j	Modal mass of mode j (bending only)
M_j^*	Generalised modal mass of mode j (bending + torsion)
$P_j(t)$	Generalised vertical modal force on mode j
$R_j(t)$	Total generalised modal force on mode j (including moment contributions)
ω_j	Natural circular frequency of mode j
ξ_j	Damping ratio of mode j
$\boldsymbol{w_j}(t)$	Reconstructed displacement for mode j ($n \times 1$)
$\boldsymbol{\theta_j}(t)$	Reconstructed torsional rotation for mode j ($n \times 1$)
w_j	Modal vertical displacement at the examined section centre of mass
θ_j	Modal rotation of the examined section
H	Generic point on the cross-section
e	Distance between H and the section centre of mass
$W_{H,j}$	Modal vertical displacement of H combining w_j and $\theta_j e$

Pedestrian Parameters

G_p	Pedestrian weight
v_s	Walking speed
f_s	Pacing frequency
T	Step period
T_c	Foot-ground contact time
Δt	Overlap time between left and right footfalls
DLF_k	Dynamic load factor of k-th harmonic
a_k, b_k	Dynamic load factor coefficients for the k-th harmonic
l_s	Step length

Experimental Application

A	Inner deck edge
B	Centre of torsional and bending stiffness
G	Centre of mass
C	Outer deck edge
$\ddot{W}_A^{\exp}$, $\ddot{W}_C^{\exp}$	Experimental peak accelerations at A, C
$\ddot{w}_A$, $\ddot{w}_G$, $\ddot{w}_C$	Numerical peak accelerations at A, G, C from the bending-only framework
$\ddot{W}_A$, $\ddot{W}_G$, $\ddot{W}_C$	Numerical peak accelerations at A, G, C from the bending-torsion framework

Multiplication Factors

α_{tors}	Torsional multiplication factor
$\alpha_{\text{pos}}(H)$	Positional multiplication factor

Acknowledgement(s)

The Oslo Municipality is sincerely acknowledged for granting permission to conduct dynamic testing on the Bumerang footbridge, enabling the experimental validation of the proposed method. The Degree of Freedom Engineering Company, designer of the aforementioned footbridge, is also gratefully acknowledged for providing valuable technical information, which facilitated the planning, execution, and post-processing of the tests. The authors also wish to thank Scott Brenna of the Mechanical and Dynamical Laboratory at the Norwegian University of Life Sciences for his valuable assistance in coordinating and supporting the experimental work.

Author contributions

CRediT: **Ghita Eslami Varzaneh**: Conceptualization, Data curation, Formal analysis, Investigation, Methodology, Software, Writing – original draft, Writing – review & editing; **Elisa Bassoli**: Conceptualization, Data curation, Investigation, Methodology, Supervision, Validation, Writing – original draft, Writing – review & editing; **Loris Vincenzi**: Conceptualization, Data curation, Investigation, Methodology, Software, Supervision, Validation, Writing – original draft, Writing – review & editing; **Angelo Aloisio**: Conceptualization, Methodology, Supervision, Validation, Writing – review & editing; **Bruno Briseghella**: Conceptualization, Methodology, Supervision, Validation, Writing – review & editing; **Roberto Tomasi**: Conceptualization, Methodology, Project administration, Supervision, Validation, Writing – review & editing.

Disclosure statement

No potential conflict of interest is reported by the author(s).

ORCID

Ghita Eslami Varzaneh http://orcid.org/0000-0002-2985-9359
Elisa Bassoli http://orcid.org/0000-0002-4919-1421
Loris Vincenzi http://orcid.org/0000-0003-2541-7104
Angelo Aloisio http://orcid.org/0000-0002-6190-0139
Bruno Briseghella http://orcid.org/0000-0002-8002-2298
Roberto Tomasi http://orcid.org/0000-0001-8002-8481

Data availability statement

The data and code supporting the findings of this study can be obtained from the corresponding author upon reasonable request.

References

Al-Smadi, Y. M., Al-Rousan, R. Z., Laradhi, A. A., & Avci, O. (2022). Vibration serviceability investigation of a curved footbridge. *Practice Periodical on Structural Design and Construction*, *27*(4), 04022040. https://doi.org/10.1061/(ASCE)SC.1943-5576.0000714

Bachmann, H., & Ammann, W. (1987). *Vibrations in structures: Induced by man and machines*. International Association for Bridge and Structural Engineering.

Bassoli, E., Gambarelli, P., & Vincenzi, L. (2018). Human-induced vibrations of a curved cable-stayed footbridge. *Journal of Constructional Steel Research*, *146*, 84–96. https://doi.org/10.1016/j.jcsr.2018.02.001

Bassoli, E., Van Nimmen, K., Vincenzi, L., & Van den Broeck, P. (2018). A spectral load model for pedestrian excitation including vertical human-structure interaction. *Engineering Structures*, *156*, 537–547. https://doi.org/10.1016/j.engstruct.2017.11.050

Bassoli, E., & Vincenzi, L. (2021). Parameter calibration of a social force model for the crowd-induced vibrations of footbridges. *Frontiers in Built Environment*, *7*, 656799. https://doi.org/10.3389/fbuil.2021.656799

Brownjohn, J. M. W., Fok, P., Roche, M., & Omenzetter, P. (2004). Long span steel pedestrian bridge at Singapore Changi Airport – Part 2: Crowd loading tests and vibration mitigation measures. *Structural Engineer*, *82*(16), 21–27.

Bruno, L., & Venuti, F. (2008). The pedestrian speed-density relation: Modelling and application. In *Proceedings of the 3rd International Conference on Footbridges* (pp. 255–256).

Bruno, L., Venuti, F., & Nascé, V. (2012). Pedestrian-induced torsional vibrations of suspended footbridges: Proposal and evaluation of vibration countermeasures. *Engineering Structures*, *36*, 228–238. https://doi.org/10.1016/j.engstruct.2011.12.012

BSI. (2008). UK National Annex to Eurocode 1: Actions on structures – Part 2: Traffic loads on bridges. NA to BS EN 1991-2:2003.

Buchmueller, S., & Weidmann, U. (2006). Parameters of pedestrians, pedestrian traffic and walking facilities. *IVT Schriftenreihe*, *132*, 1–58.

Bursi, O. S., Kumar, A., Abbiati, G., & Ceravolo, R. (2014). Identification, model updating, and validation of a steel twin deck curved cable-stayed footbridge. *Computer-Aided Civil and Infrastructure Engineering*, *29*(9), 703–722. https://doi.org/10.1111/mice.12076

Caetano, E., Cunha, A., Magalhães, F., & Moutinho, C. (2010). Studies for controlling human-induced vibration of the Pedro e Inês footbridge, Portugal. Part 1: Assessment of dynamic behaviour. *Engineering Structures*, *32*(4), 1069–1081. https://doi.org/10.1016/j.engstruct.2009.12.034

Chen, X., Geng, X., Fu, W., Tan, L., Guan, J., & Liu, T. (2024). Vibration serviceability assessment of ribbon-shaped large-span footbridge at high altitudes under wind-pedestrians coupling effects. *Structures*, *66*, 106885. https://doi.org/10.1016/j.istruc.2024.106885

da Silva, F. T., Brito, H. M. B. F., & Pimentel, R. L. (2013). Modeling of crowd load in vertical direction using biodynamic model for pedestrians crossing footbridges. *Canadian Journal of Civil Engineering*, *40*(12), 1196–1204. https://doi.org/10.1139/cjce-2011-0587

Eslami Varzaneh, G., Bassoli, E., He, L., & Vincenzi, L. (2025). Crowd-induced vibrations in a timber arch bridge. In *Proceedings of ARCH 2023* (Vol. 33, pp. 174–181). Springer Nature. https://doi.org/10.1007/978-3-031-86719-4_20

Eslami Varzaneh, G., Bassoli, E., & Vincenzi, L. (2024). A simplified method based on improved multiplication factors to assess crowd-induced vertical vibrations of footbridges. *Structure and Infrastructure Engineering*, 1–23. https://doi.org/10.1080/15732479.2024.2386456

Fenu, L., Congiu, E., Lavorato, D., Briseghella, B., & Marano, G. C. (2019). Curved footbridges supported by a shell obtained through thrust network analysis. *Journal of Traffic and Transportation Engineering (English Edition)*, *6*(1), 65–75. https://doi.org/10.1016/j.jtte.2018.10.007

Fukuchi, C. A., Fukuchi, R. K., & Duarte, M. (2019). Effects of walking speed on gait biomechanics in healthy participants: A systematic review and meta-analysis. *Systematic Reviews*, *8*(1), 153. https://doi.org/10.1186/s13643-019-1063-z

He, L., Castoro, C., Aloisio, A., Zhang, Z., Marano, G. C., Gregori, A., Deng, C., & Briseghella, B. (2022). Dynamic assessment, FE modelling and parametric updating of a butterfly-arch stress-ribbon pedestrian bridge. *Structure and Infrastructure Engineering*, *18*(7), 1064–1075. https://doi.org/10.1080/15732479.2021.1995444

Helbing, D., Buzna, L., Johansson, A., & Werner, T. (2005). Self-organized pedestrian crowd dynamics: Experiments, simulations, and design solutions. *Transportation Science*, *39*(1), 1–24. https://doi.org/10.1287/trsc.1040.0108

Helbing, D., & Molnár, P. (1995). Social force model for pedestrian dynamics. *Physical Review E*, *51*(5), 4282–4286. https://doi.org/10.1103/physreve.51.4282

HIVOSS. (2008). *Design of footbridges – Guideline*. Human Induced Vibrations of Steel Structures.

Ingólfsson, E. T., Georgakis, C. T., & Jönsson, J. (2012). Pedestrian-induced lateral vibrations of footbridges: A literature review. *Engineering Structures*, *45*, 21–52. https://doi.org/10.1016/j.engstruct.2012.05.038

ISO 10137. (2007). *Bases for design of structures – Serviceability of buildings and walkways against vibrations*.

Jiménez-Alonso, J. F., Sáez, A., Caetano, E., & Magalhães, F. (2016). Vertical crowd–structure interaction model to analyze the change of the modal properties of a footbridge. *Journal of Bridge Engineering*, *21*(8), C4015004. https://doi.org/10.1061/(asce)be.1943-5592.0000828

Li, Q., Fan, J., Nie, J., Li, Q., & Chen, Y. (2010). Crowd-induced random vibration of footbridge and vibration control using multiple tuned mass dampers. *Journal of Sound and Vibration*, *329*(19), 4068–4092. https://doi.org/10.1016/j.jsv.2010.04.013

Li, Y., Zhang, X., Wang, C., Zhang, Y., & Wei, X. (2025). Human-induced vertical vibration of a glass suspension footbridge: Experimental study and numerical analysis. *Structure and Infrastructure Engineering*, *21*(4), 656–674. https://doi.org/10.1080/15732479.2023.2230567

Lievens, K., Lombaert, G., Van Nimmen, K., De Roeck, G., & Van den Broeck, P. (2018). Robust vibration serviceability assessment of footbridges subjected to pedestrian excitation: Strategy and applications. *Engineering Structures*, *171*, 236–246. https://doi.org/10.1016/j.engstruct.2018.05.047

Lu, T. W., & Chang, C. F. (2012). Biomechanics of human movement and its clinical applications. *The Kaohsiung Journal of Medical Sciences*, *28*(2 Suppl), S13–S25. https://doi.org/10.1016/j.kjms.2011.08.004

Miyachi, K., & Nakamura, S. (2021). Cable-stayed bridge with s-curved girder: Shake hands bridge. *Structural Engineering International*, *31*(4), 504–515. https://doi.org/10.1080/10168664.2020.1870908

Mo, G., Rando, M., & Overton, K. (2019). Boomerang and Jungle pedestrian bridges in Oslo. *ce/papers*, *3*(3-4), 67–72. https://doi.org/10.1002/cepa.1028

Peeters, B., & De Roeck, G. (1999). Reference-based stochastic subspace identification for output-only modal analysis. *Mechanical Systems and Signal Processing*, *13*(6), 855–878. https://doi.org/10.1006/mssp.1999.1249

Portier, K., Tolson, J. K., & Roberts, S. M. (2007). Body weight distributions for risk assessment. *Risk Analysis*, *27*(1), 11–26. https://doi.org/10.1111/j.1539-6924.2006.00856.x

Racic, V., Pavic, A., & Brownjohn, J. M. W. (2009). Experimental identification and analytical modelling of human walking forces: Literature review. *Journal of Sound and Vibration*, *326*(1-2), 1–49. https://doi.org/10.1016/j.jsv.2009.04.020

Roda-Casanova, V., Hernández-Figueirido, D., Sancho Bru, J. L., & Martínez-Rodrigo, M. D. (2024). Numerical modelling and vibration serviceability assessment of a steel footbridge with a significant 3D dynamic behaviour. *Proceedings of the Institution of Mechanical Engineers, Part C: Journal of Mechanical Engineering Science*, *238*(3), 708–723. https://doi.org/10.1177/09544062231181827

Rodríguez-Suesca, A. E., Gutiérrez-Junco, O. J., & Hernández-Montes, E. (2022). Vibration performance assessment of deteriorating footbridges: A study of Tunja's public footbridges. *Engineering Structures*, *256*, 113997. https://doi.org/10.1016/j.engstruct.2022.113997

SETRA. (2006). *Footbridges – Assessment of vibrational behaviour of footbridges under pedestrian loading*.

Van Nimmen, K., Lombaert, G., De Roeck, G., & Van den Broeck, P. (2014). Vibration serviceability of footbridges: Evaluation of the current codes of practice. *Engineering Structures*, *59*, 448–461. https://doi.org/10.1016/j.engstruct.2013.11.006

Van Nimmen, K., Van den Broeck, P., Verbeke, P., Schauvliege, C., Mallié, M., Ney, L., & De Roeck, G. (2017). Numerical and experimental analysis of the vibration serviceability of the Bears' Cage footbridge. *Structure and Infrastructure Engineering*, *13*(3), 390–400. https://doi.org/10.1080/15732479.2016.1160133

Van Nimmen, K., Van Hauwermeiren, J., & Van den Broeck, P. (2021). Eeklo footbridge: Benchmark dataset on pedestrian-induced vibrations. *Journal of Bridge Engineering*, *26*(7), 05021007. https://doi.org/10.1061/(ASCE)BE.1943-5592.0001707

Venuti, F., Racic, V., & Corbetta, A. (2016). Modelling framework for dynamic interaction between multiple pedestrians and vertical vibrations of footbridges. *Journal of Sound and Vibration*, *379*, 245–263. https://doi.org/10.1016/j.jsv.2016.05.047

Venuti, F., & Tubino, F. (2021). Human-induced loading and dynamic response of footbridges in the vertical direction due to restricted pedestrian traffic. *Structure and Infrastructure Engineering*, *17*(10), 1431–1445. https://doi.org/10.1080/15732479.2021.1897630

Weidmann, U. (1993). Transporttechnik der Fußgänger: Transporttechnische Eigenschaften des Fußgängerverkehrs, Literaturauswertung. *IVT Schriftenreihe*, *90*, 1–87.

Zhang, Y., He, W., Zhang, J., & Dong, H. (2021). Experimental and numerical investigation on dynamic properties and human-induced vibrations of an asymmetric steel-plated stress-ribbon footbridge. *Advances in Civil Engineering*, *2021*(1), 2028378. https://doi.org/10.1155/2021/2028378

Živanović, S., Pavić, A., & Ingólfsson, E. T. (2010). Modeling spatially unrestricted pedestrian traffic on footbridges. *Journal of Structural Engineering*, *136*(10), 1296–1308. https://doi.org/10.1061/(ASCE)ST.1943-541X.0000226

Živanović, S., Pavic, A., & Reynolds, P. (2005). Vibration serviceability of footbridges under human-induced excitation: A literature review. *Journal of Sound and Vibration*, *279*(1-2), 1–74. https://doi.org/10.1016/j.jsv.2004.01.019